



Universiteit
Leiden
The Netherlands

Regulation of endosomal and phagosomal transport

Kuijl, C.P.

Citation

Kuijl, C. P. (2008, October 15). *Regulation of endosomal and phagosomal transport*. Retrieved from <https://hdl.handle.net/1887/13146>

Version: Corrected Publisher's Version

License: [Licence agreement concerning inclusion of doctoral thesis in the Institutional Repository of the University of Leiden](#)

Downloaded from: <https://hdl.handle.net/1887/13146>

Note: To cite this publication please use the final published version (if applicable).

Chapter 4

The Molecular Mechanism of Cholesterol Control of Late Endosomal Transport by Dynein Motors

Cell, submitted

THE MOLECULAR MECHANISM OF CHOLESTEROL CONTROL OF LATE ENDOSOMAL TRANSPORT BY DYNEIN MOTORS

Nuno Rocha, Coenraad Kuijl[†], Rik van der Kant^{*}, Lennert Janssen, Wilbert Zwart^{*} and Jacques Neefjes^{*}.
Division of Tumor Biology, The Netherlands Cancer Institute, Plesmanlaan 121, 1066CX Amsterdam The Netherlands

[†] Equal contribution, ^{*} Corresponding authors; email J.NEEFJES@NKI.NL; W.ZWART@NKI.NL

SUMMARY

Late endosomes and lysosomes exhibit bidirectional motility along microtubules by the alternating actions of kinesin and dynein motor proteins. The Rab7 effector RILP recruits the dynein motor to late endosomes for microtubular minus-end transport but how this complex is disassembled and what regulates the process to allow for the observed changes in direction is unclear. The Rab7-RILP complex interacts with the oxysterol-binding protein ORP1L. Here we show that the late endosomal cholesterol content determines the conformational state of ORP1L, acting as a switch to control dynein-dynactin motor complex binding to its Rab7-RILP receptor, thereby regulating the direction of transport. The cytosolic state of the cholesterol-sensing OSBP-related domain (ORD) of ORP1L exposes a FFAT motif to recruit the integral membrane protein VAP. VAP then binds to and removes the dynein-dynactin motor subunit p150^{Glued} from Rab7-RILP. The FFAT motif is not exposed when ORP1L is membrane-associated allowing dynein motor binding and transport. This regulatory mechanism is disrupted in Niemann-Pick type C disease causing the characteristic clustering of cholesterol-laden late endosomes. Thus, cholesterol acts as a molecular switch, controlling the transport of late endosomes and lysosome-related organelles.

INTRODUCTION

Late endosomes, lysosomes and lysosome-related organelles, such as the MHC class

II-containing compartment (MIIC), cytosolic granules and early melanosomes move along microtubules in a so-called bidirectional manner and in a stop-and-go fashion (Jordens et al., 2006; Wubbolts et al., 1996). This bidirectional nature of movement results from the alternate action of at least two microtubule-based motor proteins with opposite polarities. The dynein-dynactin motor is essential for minus-end (inward-directed) transport and at least two motor proteins have been implicated in plus-end transport; kinesin-1 (conventional kinesin or KIF5) and kinesin-2 (heterotrimeric kinesin or KIF3) (Brown et al., 2005; Hollenbeck and Swanson, 1990; Wubbolts et al., 1999). Although this explains bidirectional motility of late endosomes and lysosomes, it does not explain control of motor activities.

Rab GTPases specify organelle identity (Pfeffer, 2001; Zerial and McBride, 2001), making them ideal central regulators of selective motor activity. Increasing evidence implicates Rab GTPases and their effectors in the selective recruitment of motor proteins to particular vesicles (Echard et al., 1998; Hoepfner et al., 2005; Jordens et al., 2001; Jordens et al., 2005). The small GTPase Rab7 associates with late endosomal and lysosomal structures as well as to most lysosomal-related organelles (Zerial and McBride, 2001). Rab7 has multiple reported functions. The yeast Rab7 ortholog, Ypt7p, can recruit the class C VPS/HOPS complex that mediates homotypic fusion (Peterson and Emr, 2001; Seals et al., 2000; Wurmser et al., 2000). This complex probably contains a Rab7 guanine nucleotide exchange

factor, which is also an effector of the early endosomal GTPase Rab5 acting in the process of Rab5-to-Rab7 conversion and thus endosomal maturation (Rink et al., 2005). Rab7 also supports dynein motor recruitment to late endosomes by sequentially recruiting its effector RILP and then the p150^{Glued} subunit of the dynein-dynactin motor protein complex (Johansson et al., 2007; Jordens et al., 2001). Active transport of late endosomes by the dynein-dynactin motor towards the minus-end of microtubules involves an additional Rab7 effector—oxysterol-binding protein (OSBP)-related protein 1L (ORP1L) (Johansson et al., 2007). ORP1L is a member of a family of OSBP-related proteins (ORPs) and interacts with GTP-bound Rab7 via its N-terminal ankyrin repeats region (Johansson et al., 2005). ORP1L also contains a pleckstrin homology (PH) domain which binds phosphoinositides (Johansson et al., 2005), a protein-interacting FFAT (Two Phenylalanines (FF) in an Acidic Tract) motif (Loewen and Levine, 2005; Loewen et al., 2003) and a C-terminal OSBP-related domain (ORD) able to bind 25-hydroxycholesterol and possibly other cholesterol derivatives within membranes (Im et al., 2005; Suchanek et al., 2007). The FFAT motif can interact with cytosolic proteins that are embedded in the ER by a C-terminal transmembrane region, called vesicle-associated membrane protein (VAMP)-associated protein (VAP)-A and VAP-B (Loewen and Levine, 2005). VAP-A and -B can form homo- and hetero-dimers (Hama-moto et al., 2005; Nishimura et al., 1999) and interact with OSBP, an ER protein related to ORP1L, which drives ER export of proteins and lipids (Wyles et al., 2002).

The RILP-controlled recruitment of dynein motors is not only operational in late endosomes and lysosomes but in all Rab7-containing compartments tested, including specialized lysosomes like early melanosomes (Jordens et al., 2006), MHC class II-containing compartments (MIIC) (Jordens et al.,

2001), cytolytic granules (Stinchcombe et al., 2006) and phagosomes (Harrison et al., 2003; Marsman et al., 2004). This mechanism is responsible for the characteristic steady-state perinuclear distribution pattern of late endosomal compartments (Burkhardt et al., 1997; Harada et al., 1998; King et al., 2003; Vaughan et al., 2001).

How direction of transport is controlled remains unclear, although three models have been proposed. Motors of opposite polarity are reciprocally coordinated thereby preventing their simultaneous activity on a given vesicle. In this model, dynein and kinesin motors may use the dynactin stalk p150^{Glued} as a common adaptor to the Rab7-RILP receptor. The nature of the p150^{Glued}-associated motor then dictates the directionality of transport (Brown et al., 2005; Deacon et al., 2003). Alternatively, motors of opposite polarities may coexist on a given vesicle and directionality is decided in a “tug-of-war” on the cargoes (Gross et al., 2002; Muller et al., 2008). Finally, bidirectional movement can occur as a result of dynein motors being able to move in both directions on microtubules, as suggested from *in vitro* studies (Gennrich et al., 2007; Ma and Chisholm, 2002; Ross et al., 2006). In all cases, the p150^{Glued} interaction with the Rab7-RILP complex seems critical to determine motility and thus retention of late endosomal compartments in close proximity to the nucleus.

Cells overexpressing Rab7 and/or RILP show dense clustering of late endosomal vesicles around the minus-end of microtubules in the perinuclear area (Bucci et al., 2000; Jordens et al., 2001). This is the result of continuous dynein motor activity on late endosomal vesicles and possible exclusion of kinesin motor activities (Lebrand et al., 2002). Conversely, overexpression of the dominant-negative RILP variant Δ N-RILP prevents p150^{Glued} recruitment causing dispersal of late endosomal vesicles throughout the cytosol (Jordens et al., 2001).

The Rab7-RILP interaction with the p150^{Glued}

subunit may be controlled by factors altering the activity of Rab7, such as a GTPase activating protein (GAP) specific for Rab7 that would release RILP from Rab7 by stimulating GTP hydrolysis. Other factors might also be involved in the positioning and motility of late endosomes/lysosomes. Some have been hinted at in human diseases like the Niemann-Pick type C disease, which is phenotypically defined by cholesterol-laden late endosomes/lysosomes clustered around the microtubule-organizing centre at the minus-end of microtubules (Mukherjee and Maxfield, 2004). This phenotype is shared with a series of other lysosomal storage diseases including Tangier, Fabry and Gaucher disease (Maxfield and Tabas, 2005). Increasing intracellular cholesterol levels with the chemical compound U18666A mimics this phenotype (Koh and Cheung, 2006; Roff et al., 1991; Sobo et al., 2007) in a process involving Rab7 and Rab9 GTPases as well as RabGDI (Chen et al., 2008; Holtta-Vuori et al., 2000; Lebrand et al., 2002; Narita et al., 2005). Rab GTPases, cholesterol and motor protein activities may somehow be connected resulting in late endosomal/lysosomal clustering as observed in these lysosomal storage diseases.

Here, we identify cholesterol as a messenger sensed by ORP1L, a late endosomal Rab7-RILP receptor complex subunit. Cholesterol determines the conformation of ORP1L to expose a FFAT domain that recruits VAP. VAP then controls p150^{Glued}-dynein motor binding to RILP and microtubule minus-end transport of late endosomes. The characteristic clustering of late endosomes observed in Niemann-Pick type C and other lysosomal storage diseases are the result of this process.

RESULTS

Late endosomes exhibit variable timing of bidirectional stop-and-go motions.

Late endosomes, like MIIC, move along microtubules in a so-called bidirectional

manner and in a stop-and-go fashion by the action of dynein and kinesin motor proteins (Wubbolts et al., 1996). We have visualized these motions in the human melanoma cell line MelJuSo expressing Green Fluorescent Protein (GFP) tagged MHC class II using time-lapse confocal microscopy (Figure 1A). The MIIC regularly stops before continuing or switching direction of movement. The motility was subsequently plotted in a rose diagram where the speed and direction relative to the previous movement are plotted (Figure 1B). About 40% of peripheral MIIC structures were immotile during the time of analysis. The motile MIIC structures moved at $0.4 \pm 0.3 \mu\text{m/s}$ in all directions. A vesicle tends to move along a single microtubule in time, since directions are primarily forward or reverse (Figure 1B). The time a vesicle stops before moving again is plotted in Figure 1C. There appears to be no correlation between the direction before standstill and the direction after standstill (data not shown). This suggests that motor-driven vesicle transport occurs with variations in standstill, direction of movement and progression after the standstill.

Rab7 is not a substrate for the TBC1D15 when in complex with RILP.

Activated GTP-loaded Rab7 recruits its effector RILP that acts as a selective dynein motor receptor on late endosomal membranes by binding the p150^{Glued} subunit of the dynactin complex (Johansson et al., 2007). Inactivation of Rab7 by a Rab7-specific GTPase-activating protein could control dynein motor recruitment to late endosomes. We selected nine GAPs to generate shRNA constructs (Figure S1) which were introduced in MelJuSo cells expressing GFP-Rab7. Since GFP-Rab7 cycles between a membrane-associated GTP-bound active and a cytosolic inactive GDP-bound state, the Rab7 cycle can be monitored by photobleaching experiments (Jordens et al., 2001) (Figure 2A). Only downregulation of the RabGAP

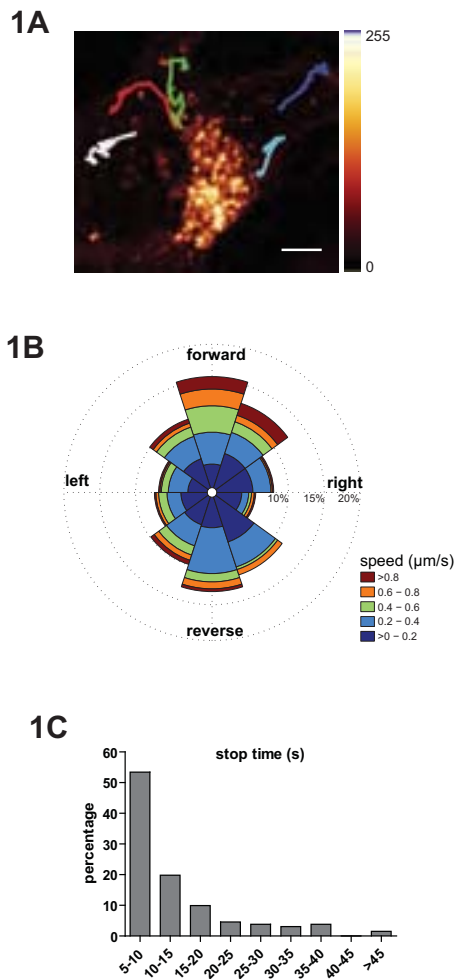


Figure 1. Analyses of MIIC stop-and-go bidirectional motility.

(A) Tracking of MHC class II vesicle (MIIC) movement. The stably transfected GFP-HLA-DR1 MeJuSo cell line was imaged by time-lapse confocal microscopy with images taken every 5 s over a period of 195 s (see also Supplemental Movie M1). The positions of five vesicles moving in the confocal section were projected and illustrate the variability in MIIC movement. The velocity of the vesicles, the stop-time and the angle of movement following the stop-time were derived from similar images. (B) The velocity of vesicles was determined in the stable GFP-HLA-DR1 MeJuSo cell line. Vesicle velocity and direction relative to the previous direction from 36 tracks (820 data points) were quantified and plotted in a rose diagram. Each segment of 36 degrees (total 360 degrees) shows the direction of movement. Each segment is subdivided into 5 discrete compartments indicating the speed of vesicle movement in that direction. (C) Vesicles stop before continuing or switching direction. The stop time (standstill) was determined from 36 tracks analyzed and binned over 5 s intervals. Total stop times were set at 100%.

TBC1D15 by shRNA quenched the Rab7 cycle in living cells (Figures 2B and 2C). The TBC (Tre-2/Bub2/Cdc16) domain, a conserved catalytic domain that specifies most RabGAPs (Albert et al., 1999; Bernards, 2003), of TBC1D15 was subsequently expressed, isolated and tested in an in vitro GTPase assay with [γ - 32 P-GTP]-loaded Rab7 (Figure 2D). Consistent with recent data, we found that the TBC domain of TBC1D15 stimulated the low intrinsic GTPase activity of Rab7 (Zhang et al., 2005). To test whether this was also the case when Rab7 was complexed to RILP and ORP1L (Johansson et al., 2005; Johansson et al., 2007) we isolated RILP and ORP1L. Complexes of [γ - 32 P-GTP]-

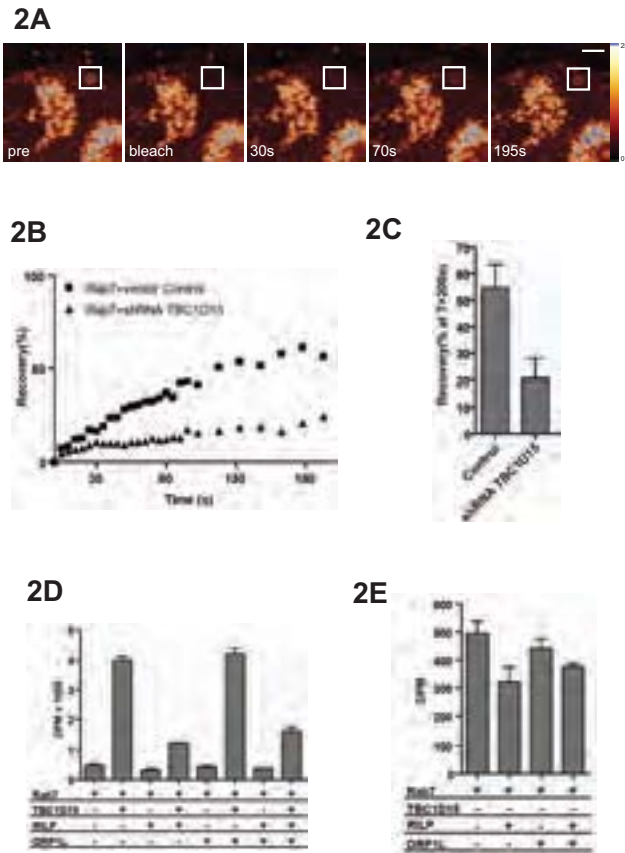
loaded Rab7 with RILP and/or ORP1L were assembled prior to adding the TBC domain of TBC1D15 to the reactions (Figure 2D). RILP but not ORP1L decreased the GTPase activity of Rab7 and TBC1D15. Simultaneous binding of RILP and ORP1L to [γ - 32 P-GTP]-loaded Rab7 did not further decrease GTPase activation of Rab7. This suggests that RILP limits access of TBC1D15 to Rab7 further slowing down the already slow Rab7 GTPase cycle (Figures 2B and 2S). The rapid mechanism of directional switching observed in late endosomal transport (Figures 1A and 1C) is therefore unlikely controlled by TBC1D15 since RILP delays the already slow intrinsic GTPase activity of Rab7 in vitro and in living cells (Jordens et al., 2001).

ORP1L controls p150^{Glued} binding to Rab7-RILP and late endosomal positioning.

ORP1L binds to Rab7-RILP via its N-terminal ankyrin repeats and is required for regulation of late endosomal transport by

Figure 2. RILP prevents Rab7 GTPase activation by Rab7GAP.

(A) The GFP-Rab7 cycle in living MeJuSo cells as determined by FRAP. GFP-Rab7-positive vesicles in living MeJuSo cells were photobleached and the recovery of fluorescence was followed in time. Single frames corresponding to a typical sequence with a GFP-Rab7-positive vesicle (inside white-box) prior to bleaching (pre), immediately after bleaching (bleach), and post-bleaching after different time intervals (30s, 70s, and 195s) are shown. (B) Quantification of fluorescence recovery of GFP-Rab7 on vesicles in living MeJuSo cells expressing a control shRNA or a shRNA for TBC1D15, as indicated. Nine potential RabGAPs (Figure S1) were tested with only one affecting the GFP-Rab7 cycle. shRNA-mediated silencing of TBC1D15 quenched the GFP-Rab7 cycle and the bleached membrane-bound Rab7 was less efficiently exchanged for fluorescent GFP-Rab7. (C) The recovery of fluorescence of GFP-Rab7 on vesicles in living MeJuSo cells expressing control or shRNA for the TBC1D15 was determined after 200 s. The cycle time of GFP-Rab7 was not significantly affected by intracellular localization but was strongly decreased by silencing Rab7GAP. The means and SD from five independent experiments are plotted. (D) RILP inhibits stimulation of the Rab7 GTPase activity by TBC1D15. $\gamma^{32}P$ -GTP hydrolysis by purified GST-Rab7 was monitored in an in vitro reaction in the presence or absence of purified RILP, ORP1L and Rab7GAP, as indicated. The means and SD of duplicates in two independent experiments are shown. (E) Zoom-in on the effects of RILP and ORP1L on the intrinsic GTPase activity of Rab7 illustrating that RILP slows the intrinsic Rab7 GTPase activity. The means and SD of duplicates in two independent experiments are shown.



the dynein motor (Johansson et al., 2005; Johansson et al., 2007). To test which ORP1L domains are involved in late endosomal transport control, we constructed a series of C-terminal truncations of ORP1L fused to the monomeric Red Fluorescent Protein mRFP (Shaner et al., 2004) (Figure 3A) and co-expressed these with GFP-RILP in MeJuSo cells. Cells were fixed and stained for p150^{Glued}. Removal of the C-terminal ORD (Δ ORD) prevented p150^{Glued} recruitment by RILP resulting in relocation of

RILP-containing compartments to the cell periphery, further C-terminal truncations allowed p150^{Glued} binding to RILP and clustering at the minus-end of microtubules (Figure 3B). To test whether the ORD is directly involved in excluding p150^{Glued} binding to RILP, this domain was exchanged for two ORP1L PH domains in tandem (Δ ORDPHDPHD). Tandem PH domains increase the avidity of binding to phosphoinositides considerably (Lemmon and Ferguson, 2000) and were used to mimic the ORD in a mem-

brane-associated state. The Δ ORDPHDPHD chimera allowed p150^{Glued} recruitment by RILP resulting in the clustering of RILP-positive compartments at the minus-end of microtubules (Figure 3B).

Thus, ORP1L allowed p150^{Glued} binding to RILP, unlike the mutant only lacking the cholesterol-interacting domain ORD. Further C-terminal truncations restored p150^{Glued} recruitment by RILP. This would fit a model where the ORD exists in two conformational states: a membrane-associated 'down' state when the ORD binds cholesterol, and a cytosolic-exposed 'up' state when not interacting with such sterols on late endosomal membranes. In the 'up' state, exposure of a region between the PH domain and the ORD would then affect binding of p150^{Glued} to Rab7-RILP. This region is exposed in Δ ORD and prevents p150^{Glued}-RILP interactions whereas further C-terminal truncations eliminates this and restore the p150^{Glued}-RILP interaction (Figure 3B). Substitution of the ORD by tandem PH domains would impose a 'down' state conformation thereby preventing the exposure of the region between the PH domain and the ORD. Binding of p150^{Glued} to Rab7-RILP is then restored and RILP-containing compartments clustered as the result of prolonged p150^{Glued}-dynein motor binding to Rab7-RILP complexes (Figure 3B).

The ORP1L region between the PH domain and ORD (aa 408-514) then controls access of p150^{Glued} to RILP. This region contains a predicted coiled-coil region (aa 430-463) (Johansson et al., 2007) followed by a FFAT motif (aa 472-482; SEDEFYDALSD) (Loewen et al., 2003) (Figure 3A). This FFAT motif is present in other ORP1L family members where it mediates interactions with Vesicle associated membrane (VAMP)-Associated Proteins (VAP) (Lehto et al., 2005; Wyles et al., 2002). To assess whether the FFAT motif is involved in excluding p150^{Glued} from RILP, an inactivating point mutation (D478A) in the FFAT

motif (Loewen et al., 2003) was introduced in mRFP- Δ ORD. This mutant was co-expressed with GFP-RILP in cells before fixation and staining for p150^{Glued} (Figure 3C). Whereas Δ ORD excluded RILP-mediated recruitment of p150^{Glued} resulting in vesicle scattering, the single point mutation in the FFAT motif, Δ ORDFFAT(D478A), rescued p150^{Glued} binding to RILP and clustering of RILP-positive compartments.

Cholesterol affects ORP1L conformation and positioning of late endosomes.

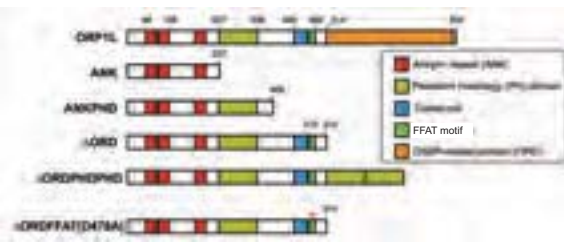
The FFAT motif preceding the cholesterol-sensing domain ORD is apparently involved in excluding p150^{Glued}-dynein motor binding to the Rab7-RILP receptor. This motif could be exposed when the ORD adopts a cytosolic position as reflected by Δ ORD and shielded when the ORD is membrane-bound as reflected by Δ ORDPHDPHD. Recent studies suggest that OSBP/ORPs are involved in non-vesicular transport of sterols between specific donor and acceptor membranes through a functional cycle that involves ORD-dependent extraction of sterols from membranes and reciprocal conformational changes (Im et al., 2005; Lehto et al., 2008; Yang, 2006). The ORD is a cholesterol-interacting and extracting domain and it may adopt a membrane-bound conformation when extracting cholesterol from donor membranes, and a cytosol-exposed conformation following cholesterol extraction. If so, cholesterol would determine the orientation of the ORD relative to membranes and the exposure of the preceding FFAT motif. Late endosomal cholesterol content would then determine ORP1L conformation and vesicle positioning by regulating binding of p150^{Glued}-dynein motors to Rab7-RILP receptors

The intracellular cholesterol content of MeJuSo cells was manipulated to assess the role of cholesterol in ORP1L-mediated regulation of Rab7-RILP-p150^{Glued}-dynein motor transport of late endosomes. Cells

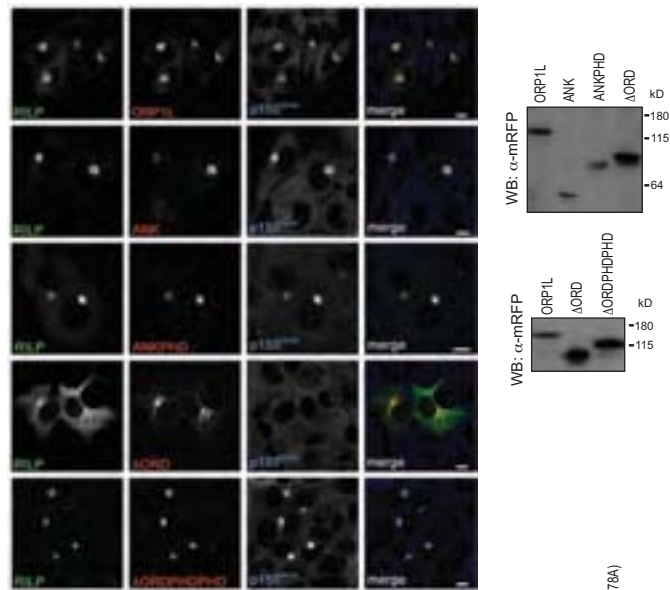
Figure 3. ORP1L controls recruitment of p150^{Glued} to the Rab7-RILP receptor.

(A) ORP1L domain structure and constructs. Five domains can be distinguished in ORP1L. A series of C-terminal truncation mutants were generated. Numbers indicate amino acid residue positions. All constructs were N-terminally tagged with mRFP. The Δ ORDPHD- Δ PHD chimera had the ORD exchanged for a tandem PH domain derived from ORP1L. The Δ ORDFFAT(D478A) mutant was obtained by inserting a point mutation (D478A) in the FFAT motif of Δ ORD (marked by an asterisk). (B) Effect of ORP1L deletion or chimeric constructs on RILP-mediated p150^{Glued} recruitment. Left panel: MelJuSo cells were transfected with GFP-RILP and mRFP-ORP1L constructs prior to immunofluorescence confocal microscopy with anti-p150^{Glued} antibodies. n>200 for each condition. Scale bars, 10 μ m. Right panels: MelJuSo cells were transfected with the indicated mRFP-ORP1L, -ANK, -ANKPHD, - Δ ORD, and - Δ ORDPHD constructs and whole-cell lysates were analyzed by SDS-PAGE and Western blotting with anti-mRFP antibodies (WB: α -mRFP). (C) Effect of mutating the FFAT motif in Δ ORD on RILP-mediated p150^{Glued} recruitment. Left panel: MelJuSo cells transfected with GFP-RILP and mRFP- Δ ORD carrying an inactivating point mutation in its FFAT motif, Δ ORDFFAT(D478A), show clustering of RILP-positive compartments by immunofluorescence confocal microscopy with anti-p150^{Glued} antibodies. n>200. Scale bar, 10 μ m. Right panel: MelJuSo cells were transfected with the indicated mRFP- Δ ORD or mRFP- Δ ORDFFAT(D478A) constructs and whole-cell lysates were subjected to immunoblot analysis using anti-mRFP antibodies (WB: α -mRFP).

3A



3B



3C



were cultured in normal serum (FCS)-containing medium (F-medium), in delipidated serum-containing medium supplemented with a statin (Lovastatin) which inhibits 3-hydroxy-3-methylglutaryl coenzyme A (HMG-CoA) reductase and thus blocks en-

dogenous cholesterol synthesis (S-medium), or in FCS-containing medium supplemented with U18666A (U-medium), a drug causing cholesterol accumulation in late endosomal compartments (Sobo et al., 2007; Sugii et al., 2006). Cells were fixed and cholesterol de-

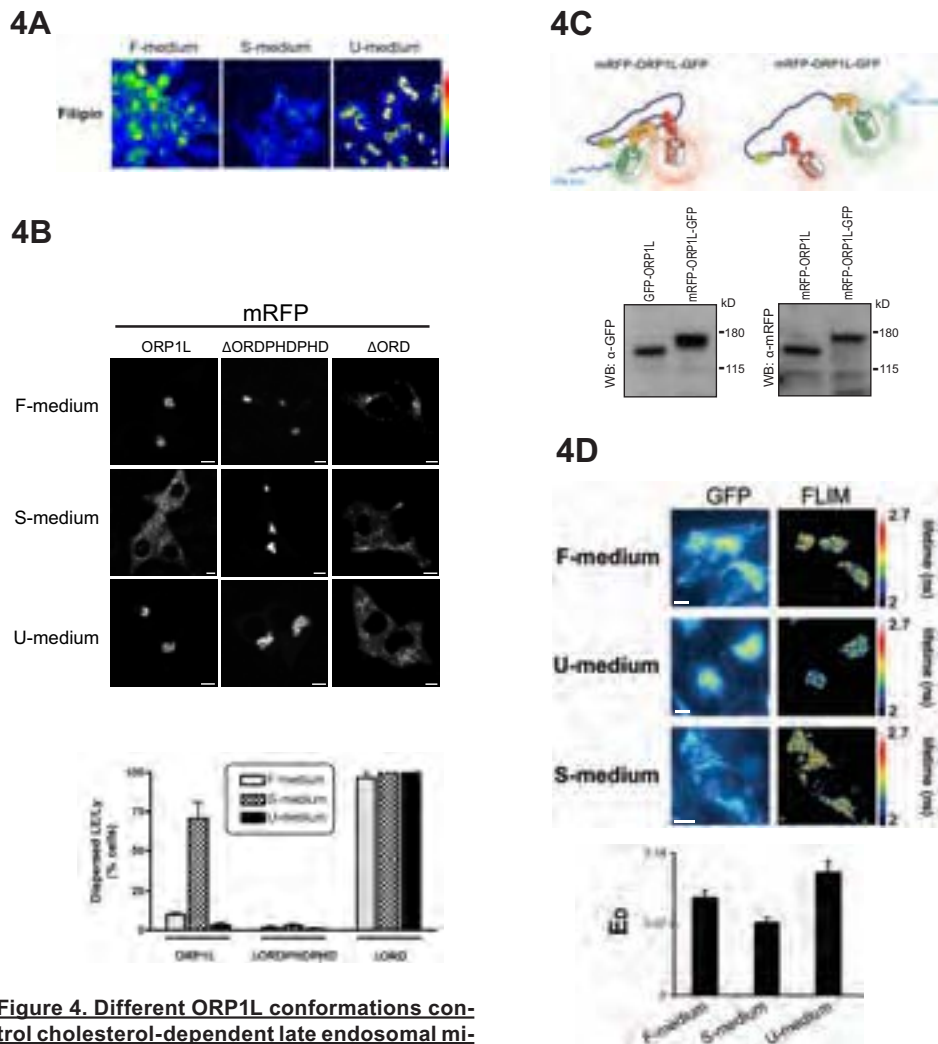


Figure 4. Different ORP1L conformations control cholesterol-dependent late endosomal minus-end transport and positioning. (A) Modulation of intracellular cholesterol. MeJuSo cells were cultured in normal (F-medium), cholesterol-depleted medium supplemented with Lovastatin to block synthesis of endogenous cholesterol (S-medium) or in normal medium supplemented with U18666A (U-medium) which elicits cholesterol accumulation in late endosomal compartments. Cells were fixed and stained with filipin to detect cholesterol. Images were obtained using identical settings on the microscope. A colour LUT is applied to illustrate the differences in filipin staining and cholesterol in cells. $n > 100$ for each condition. Scale bars, $10\mu\text{m}$. (B) ORP1L controls cholesterol-dependent vesicle positioning. MeJuSo cells expressing mRFP-ORP1L, Δ ORDPHDPHD or Δ ORD were cultured in normal (F-medium), medium decreasing (S-medium) or enhancing (U-medium) intracellular content of cholesterol. ORP1L-bearing vesicles disperse in S-medium treated cells unless the cholesterol-insensitive ORP1L variant Δ ORDPHDPHD is expressed. Scale bars, $10\mu\text{m}$. Bar chart shows the percentage of cells showing dispersed late endosomes/lysosomes (LE/Ly) under the different cholesterol-manipulating treatments, as indicated. The means and SD from 150 cells analyzed in three independent experiments for each condition are shown. (C) Concept of intramolecular FRET for mRFP-ORP1L-GFP. Top: The intramolecular ORP1L FRET probe was created by tagging of ORP1L with mRFP and GFP at the N- and C-terminus, respectively. The lifetime of GFP is determined by excitation with 488 nm light. The GFP lifetime decreases when energy

is transferred from GFP to mRFP which is dependent on the distance and orientation between the two fluorophores. From this lifetime the donor FRET efficiency E_D is calculated. Bottom: Immunoblotting analyses of whole-cell lysates of MelJuSo cells stably expressing mRFP-ORP1L-GFP or transiently expressing GFP-ORP1L or mRFP-ORP1L, as indicated, using anti-GFP (WB: α -GFP) and anti-mRFP (WB: α -mRFP) antisera. (D) Cholesterol affects the conformation of ORP1L. MelJuSo cells expressing the intramolecular mRFP-ORP1L-GFP FRET probe were treated with control (F-medium), cholesterol-enhancing (U-medium) or -depleting (S-medium) conditions prior to imaging with a wide-field FLIM microscope. Left panel: GFP fluorescence as detected by wide-field microscopy and lifetime as detected by FLIM. The colour LUT depicts the different lifetimes detected. Scale bars, 10 μ m. Right panel: Donor FRET efficiency (E_D) as calculated from images as shown in the Left panel. The mean and SD from three independent experiments (70 cells analyzed for each condition) are shown.

tected by filipin staining (Bornig and Geyer, 1974) (Figure 4A).

Filipin labelled the plasma membrane and intracellular vesicles. Labelling was respectively decreased or markedly increased under cholesterol-depleting (S-medium) or -enhancing (U-medium) treatments. Cells transiently expressing mRFP-ORP1L, Δ ORD or Δ ORDPHDPHD were cultured in F-, S-, or U-medium (Figure 4B). Late endosomal structures labelled by ORP1L, unlike those labelled by Δ ORDPHDPHD, scattered in the cytosol under cholesterol-depleting conditions (S-medium). Under cholesterol-enhancing conditions (imposed by U18666A in the U-medium), ORP1L-labelled vesicles, unlike Δ ORD labelled vesicles, clustered in a perinuclear region (Figure 4B; quantification data in bar chart).

To determine whether late endosomal cholesterol content indeed affected the conformation of ORP1L, a mRFP-ORP1L-GFP fusion protein was expressed in MelJuSo cells to monitor intramolecular Fluorescence Resonance Energy Transfer (FRET). FRET is the radiationless energy transfer from a donor fluorophore to a suitable acceptor (Förster, 1948). This is affected by alterations in distance or orientation between GFP and mRFP (Calleja et al., 2003; Förster, 1948) and thus reveals conformational changes within ORP1L. FRET was determined by fluorescence lifetime imaging microscopy (FLIM) on living cells cultured at 37°C, where the fluorescence lifetime of the donor fluorophore, GFP, is measured. The lifetime of GFP is typically 2,7 ns (Pep-

perkok et al., 1999), but decreases in the case of FRET, when energy is transferred to the acceptor fluorophore, mRFP (Figure 4C). As internal control, the cells were co-cultured with MelJuSo cells expressing Histone2B-GFP only. FLIM was determined in cells stably expressing mRFP-ORP1L-GFP under control (F-medium), cholesterol-depleting (S-medium), or -enhancing (U-medium) conditions. The donor FRET efficiencies (E_D) (calculated from the GFP lifetimes) were affected by the different cholesterol-manipulating treatments (Figure 4D), suggesting that cholesterol content variations in late endosomal compartments elicit different ORP1L conformations.

These results demonstrate that the Rab7-RILP interacting protein ORP1L uses its ORD to sense variations in cholesterol content. Cholesterol concentrations affect ORD conformation and exposure of the FFAT motif that is critical for preventing the interaction of the dynein motor subunit p150^{Glued} with its receptor Rab7-RILP, and thereby determine late endosomal vesicle positioning.

ORP1L and Niemann-Pick type C disease.

Various lysosomal storage diseases characteristically accumulate cholesterol in late endosomal compartments clustered at the microtubular minus-end in a perinuclear area. Best characterized is Niemann-Pick type C (NPC) where usually the multispinning membrane late endosomal protein NPC protein 1 (NPC1) is mutated or deleted (Carstea et al., 1997). NPC1 binds 25-hydroxycholes-

terol and other sterols (Infante et al., 2008a) but it is unclear whether it actually transports these over the late endosomal limiting membrane like another multispansing membrane protein ATP-binding cassette transporter A1 (ABCA1) (Chen et al., 2001). ABCA1 may expose the high cholesterol content in the lumen of late endosomes in Niemann-Pick C cells to the cytosolic leaflet of these compartments. ORPIL would then sense this cholesterol resulting in effects on Rab7-RILP-p150^{Glued}-dynein motor-mediated transport and clustering of late endosomes. siRNA-mediated downregulation of NPC1 in MelJuSo cells induced clustering of CD63-positive vesicles in the perinuclear area (Figure 5A) that accumulate cholesterol (Figure 5B), as characteristic for Niemann-Pick C disease. To test whether late endosomal cholesterol increase—as a result of NPC1 downregulation—was sensed by ORPIL, intramolecular FRET between the two extremities of mRFP-ORPIL-GFP was measured by FLIM in control or NPC1 siRNA-transfected MelJuSo cells (Figure 5C). The GFP-lifetime of mRFP-ORPIL-GFP decreased (donor FRET efficiency E_D increased) when NPC1 was downregulated by siRNA, suggesting that ORPIL adopts a different conformation in the absence of NPC1. The calculated donor FRET efficiencies (E_D) for mRFP-ORPIL-GFP in NPC1-downregulated cells are similar to those observed with U-medium treatment, which phenomimics NPC1 deficiency (Koh and Cheung, 2006; Sobo et al., 2007) (Figure 4D).

The increase in cholesterol caused by siRNA-mediated downregulation of NPC1 may be sensed by ORPIL and translated into Rab7-RILP-controlled dynein motor transport thus initiating late endosomal clustering. If so, the deletion mutant of ORPIL lacking the cholesterol-interacting domain (Δ ORD) should prevent late endosomal clustering following downregulation of NPC1. To test this, MelJuSo cells were transfected with siRNA for NPC1 along with various

mRFP-labelled ORPIL constructs, as indicated (Figure 5D). Cells were fixed and stained for NPC1 and the late endosomal marker CD63 (Infante et al., 2008b; Patel et al., 1999). NPC1 was efficiently downregulated since only nuclear background staining with the NPC1 antibody was observed. Whereas ORPIL and Δ ORDPHDPHD efficiently clustered the CD63-positive late endosomes, these compartments left the microtubule minus-end when Δ ORD was expressed. This was also observed in MelJuSo cells treated with U18666A, a compound that phenomimics Niemann-Pick type C (Figure 5E).

Despite their redistribution to the cell periphery, Δ ORD-bearing vesicles still showed accumulation of cholesterol following siRNA-mediated silencing of NPC1 (Figure 5F). This suggests that the accumulation of cholesterol observed in NPC1-deficient cells is not a result but a cause of late endosomal clustering.

The characteristic clustering of cholesterol-laden late endosomal compartments at the microtubule minus-end, as typical in Niemann-Pick type C and other lysosomal storage diseases, is the result of cholesterol sensing by ORPIL. ORPIL transmits this signal to the Rab7-RILP-p150^{Glued}-dynein motor complex for microtubule minus-end driven vesicle transport and clustering.

To examine if ORPIL significantly contributes to the control of cholesterol levels in late endosomes or is it primarily using cholesterol to control Rab7-RILP-mediated p150^{Glued}-dynein motor transport without influencing its cholesterol levels, MelJuSo cells were transfected with mRFP-ORPIL or mRFP- Δ ORDPHDPHD, fixed and labelled with filipin to detect cholesterol (Figure 5G). Overexpressing Δ ORDPHDPHD did not significantly alter cholesterol levels in late endosomal structures. This suggests that ORPIL uses cholesterol as a messenger rather than contributing directly to the intracellular distribution of cholesterol.

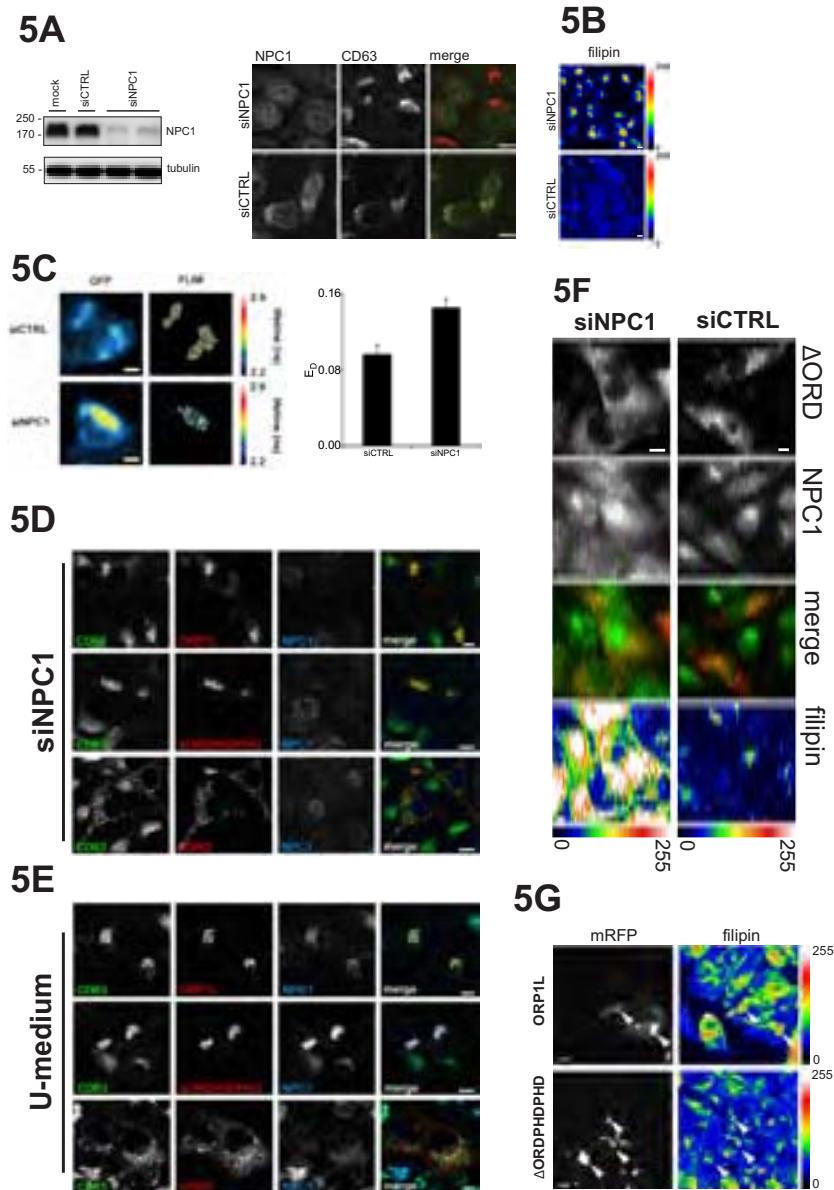


Figure 5. ORP1L conformations control late endosomal clustering in Niemann-Pick type C cells. (A) siRNA-mediated knockdown of NPC1. Left panel: whole-cell lysates of MelJuSo cells treated with transfection reagent only (mock) or with a control siRNA (siCTRL) or siRNA for NPC1 (siNPC1) were subjected to immunoblotting with anti-NPC1 and as reference anti-tubulin antibodies. Right panel: MelJuSo cells transfected with control siRNA (siCTRL) or siRNA for NPC1 (siNPC1), as indicated, prior to immunofluorescence confocal microscopy with anti-CD63 and anti-NPC1 antibodies. For siNPC1-treated cells, only background levels of anti-NPC1 antibody were detected with nuclear levels higher than vesicular levels. $n > 100$ for each condition. Scale bars, 10 μm . (B) siRNA-mediated silencing of NPC1 and intracellular cholesterol. MelJuSo cells were transfected with control (siCTRL) or NPC1 siRNA (siNPC1) prior to fixation and staining with filipin. Images were made under identical settings and a colour LUT is applied to illustrate differences in intensities. $n > 200$ for each condition. Scale bars, 10 μm . (C) siRNA-mediated si-

lencing of NPC1 elicits different ORP1L conformations. Intramolecular FRET for mRFP-ORP1L-GFP was determined by FLIM in MeJuSo cells pre-treated with control (siCTRL) or NPC1 (siNPC1) siRNAs. Left panel: GFP fluorescence detected the distribution of the ORP1L-containing vesicles by wide-field microscopy. GFP lifetime was detected by FLIM. The lifetime was determined (in ns) and plotted in false colours. Colour relates to the lifetime (in ns) as indicated in the colour LUT. Scale bars, 10 μ m. Right panel: The donor FRET efficiencies (ED) as calculated from the FLIM data. The mean and SD from 75 cells analyzed in three independent experiments are shown. (D) The ORD of ORP1L is critical for late endosomal clustering following NPC1 silencing. MeJuSo cells pre-treated (for 48 hr) with siRNA for NPC1 (siNPC1) were transfected with mRFP-tagged ORP1L, ORP1L lacking the ORD (Δ ORD) or with this domain replaced for a tandem PH domain (Δ ORDPHDPHD), prior to immunofluorescence confocal microscopy with anti-CD63 and anti-NPC1 antibodies, as indicated. $n > 200$ for each condition. Scale bars, 10 μ m. (E) The ORD of ORP1L is critical for the late endosomal characteristic clustering caused by U18666A treatment. MeJuSo cells were transfected with mRFP-tagged ORP1L, ORP1L lacking the ORD (Δ ORD) or with this domain replaced for a tandem PH domain (Δ ORDPHDPHD) and cultured in U-medium (contains U18666A) prior to immunofluorescence confocal microscopy with anti-CD63 and anti-NPC1 antibodies, as indicated. $n > 200$ for each condition. Scale bars, 10 μ m. (F) Cholesterol accumulation in NPC1-deficient cells is not a result of late endosomal clustering. MeJuSo cells pre-treated (for 48 hr) with a control siRNA (siCTRL) or siRNA for NPC1 (siNPC1) were transfected with mRFP- Δ ORD. At 24 hr post-transfection, cells were fixed and stained with anti-NPC1 antibodies and filipin to detect cholesterol. Except for the mRFP signal in the siNPC1 series (enhanced to detect the nuclear background anti-NPC1 staining), identical settings were used to produce the images. Merge shows only mRFP- Δ ORD and anti-NPC1 antibody fluorescence signals. A colour LUT is applied to illustrate differences in filipin staining. $n > 50$ for each condition. Scale bars, 10 μ m. (G) Intracellular cholesterol levels are not affected by the ORD of ORP1L. MeJuSo cells were transfected with mRFP-ORP1L or mRFP- Δ ORDPHDPHD and cultured under normal conditions (F-medium) prior to fixation and staining with filipin, as indicated. A colour LUT is applied to visualize intensities in filipin staining. Arrowheads indicate some of the transfected cells. $n > 100$ for each condition. Scale bars, 10 μ m.

ORP1L conformation, recruitment of VAP and removal of the p150^{Glued}-dynein motor.

The FFAT motif in ORP1L is critical for p150^{Glued} binding to RILP (Figure 3C). This FFAT motif in the ORP1L homologue OSBP interacts with ER proteins VAP-A and VAP-B, which regulates protein and lipid export from the ER (Loewen and Levine, 2005; Wyles et al., 2002). VAP-A and -B can form heterodimers (Hamamoto et al., 2005). To test whether VAP is involved in controlling recruitment of p150^{Glued} to RILP, MeJuSo cells were transfected with Δ ORD and RILP. In these cells, VAP-A was silenced by siRNA. Subsequently, cells were fixed and stained for p150^{Glued} (Figure 6A). Impaired recruitment of p150^{Glued} to RILP by Δ ORD co-expression could be restored by silencing the expression of VAP-A. Identical results were obtained when VAP-B was silenced (data not shown), which was expected since VAP-A and -B can form heterodimers

(Hamamoto et al., 2005). This suggests that VAP-A and -B are critical for translating the inhibitory effect of Δ ORD to p150^{Glued} recruitment of RILP.

VAP-A and -B are cytosolic proteins with a hydrophobic C-terminus embedded in the ER membrane and thus not obvious candidates for regulating transport processes in late endosomes. We tested whether VAP-A and -B could appear on late endosomes dependent on ORP1L. MeJuSo cells were transfected with YFP-tagged VAP-A or -B in the presence of CFP-RILP and mRFP- Δ ORD or mRFP- Δ ORDPHDPHD. Cells were fixed and stained for VAP and p150^{Glued} before analyses by CLSM (Figure 6B). VAP-A (and -B, data not shown) accumulated on late endosomes only when the FFAT motif was exposed as with mRFP- Δ ORD. This suggests that the cholesterol content of vesicles determines the exposure of the FFAT motif of ORP1L and thereby the recruitment of VAP.

To follow how VAP is recruited to late endosomes, photoactivatable (PA)-GFP tagged VAP-A was expressed with various mRFP-tagged ORP1L constructs in MelJuSo cells. VAP-A/PA-GFP was photoactivated in the ER with 405 nm light, at the position of the nucleus with ER structures underneath and on top, preventing activation of any VAP-A/PA-GFP already present on the vesicles. This was verified by a Z-stack projection of the cell analyzed (Figure 6C). The transfer of VAP-A to the mRFP- Δ ORD-, -ORP1L- or - Δ ORDPHDPHD-labelled late endosomes was followed by time-lapse microscopy (Figure 6C, Supplemental movie M2-4). VAP-A photoactivated at the ER swiftly accessed late endosomes labelled by mRFP- Δ ORD or -ORP1L but not - Δ ORDPHDPHD. This suggests that the conformation of ORP1L determines VAP-A recruitment to late endosomes. The exact mechanism is unclear but transfer could be inhibited when cells were cultured at 4°C (data not shown).

VAP is recruited to late endosomes by ORP1L and is involved in p150^{Glued} exclusion. To test how VAP affects p150^{Glued} binding to RILP, the reaction was reconstituted with purified proteins. The [GTP-loaded]-Rab7-RILP complex was generated to which either ORP1L or the C-terminus of p150^{Glued} (C25) were added before VAP-A was titrated into the reaction (Figure 6D, left panels). VAP-A removed C25 from the Rab7-RILP complex. ORP1L is not required for direct removal of C25 under in vitro conditions. However, ORP1L is essential in vivo to recruit VAP-A to the RILP-p150^{Glued} complex for subsequent motor removal (Fig 6CD). To test whether VAP-A directly interacted with the C25-fragment of p150^{Glued}, GST/VAP-A or GST (as a control) was bound to GST-beads and purified C25 added. A direct interaction between VAP-A and the C-terminal p150^{Glued} fragment was detected (Figure 6D, right panel). This in vitro reconstitution experiment reveals that we have defined a minimal unit controlling dynein motor bind-

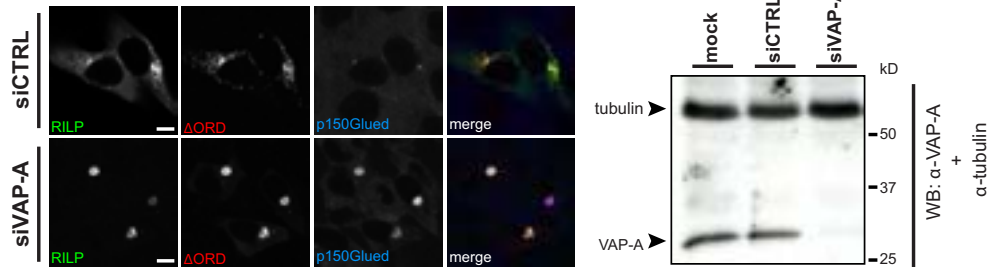
ing to late endosomes with Rab7, RILP, ORP1L, p150^{Glued} and VAP. ORP1L is required to recruit VAP in a cholesterol-dependent manner to the Rab7-RILP complex and VAP then binds to and removes the dynein motor subunit p150^{Glued} from the Rab7-RILP receptor.

DISCUSSION

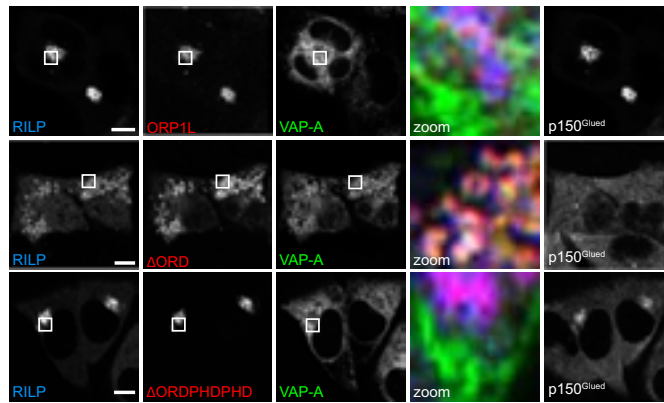
Cholesterol is a hydrophobic molecule essential for fluidity and microdomain formation in biomembranes. Although cells produce cholesterol in the ER, most cholesterol is acquired by uptake of HDL or LDL particles by the LDL receptor for transport to late endosomes and lysosomes (Ikonen, 2008). Most cholesterol is stored in the internal vesicles of multivesicular bodies for later transport to other cellular compartments (Mobius et al., 2003). Transfer of cholesterol over membranes requires transporters like ABCA1 and possibly NPC1 (Ikonen, 2008) and further transfer specific chaperones. A series of proteins with cholesterol-binding domains, like StAR-related lipid transfer (StART) domain and ORD, have been identified in various compartments to ensure correct cholesterol distribution in cells (Holthuis and Levine, 2005). Two such proteins, MLN64 and ORP1L, are located in late endosomes. MLN64 is a tetraspanin with a cytosolic StART domain and ORP1L a Rab7-interacting protein with an ORD (Ikonen, 2008).

High cholesterol content in late endosomes is typical for a series of lysosomal storage diseases with characteristic late endosomal clustering at the minus-end of microtubules. This suggests that cholesterol influences late endosomal transport in a process involving Rab GTPases, for which the precise mechanisms remain unknown (Holttä-Vuori et al., 2000). Vesicles are transported to the microtubule minus-end by the dynein-dynactin motor which is recruited to late endosomes by first binding the late endosomal specific Rab7-RILP receptor and then—supported

6A



6B



6C

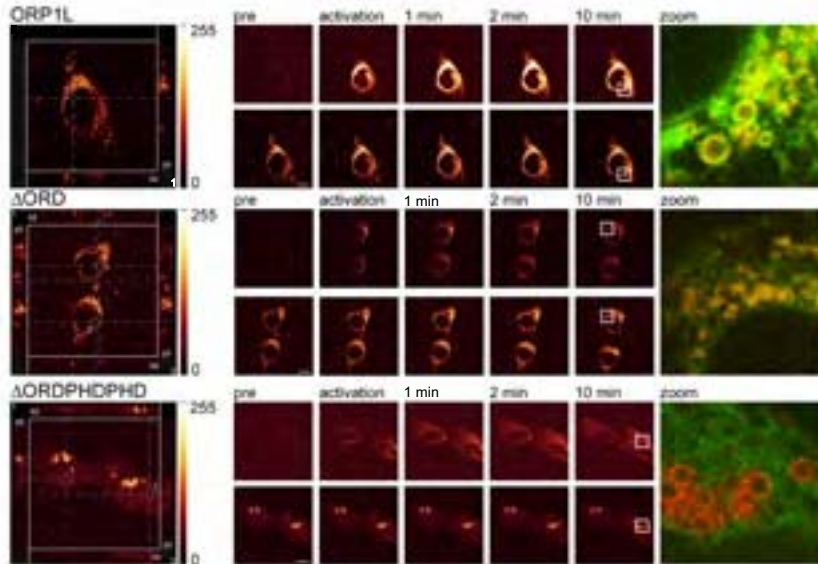
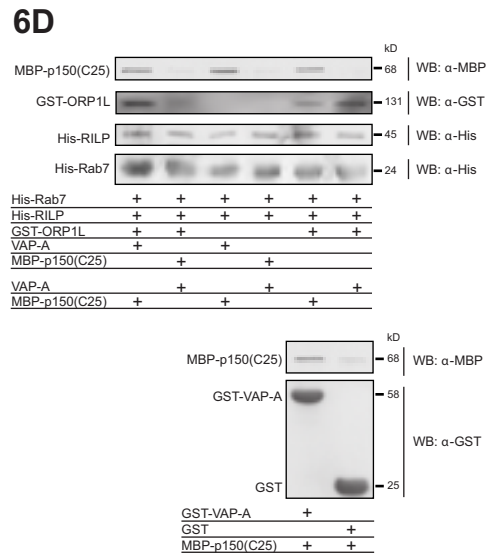


Figure 6. ORP1L recruits VAP to bind and remove p150^{Glued} for Rab7-RILP. (A) p150^{Glued} exclusion by Δ ORD and VAP-A. VAP-A was silenced by siRNA in cells expressing GFP-RILP and mRFP- Δ ORD. Top: Cells were fixed and stained for p150^{Glued} before analyses by confocal microscopy. $n > 100$ for each condition. Scale bars, 10 μ m. Bottom: Western blot analyses of cells transfected with transfection reagent only (mock), control (siCTRL) or VAP-A siRNA (siVAP-A) and subjected to immunoblotting with α -VAP-A and α -tubulin (as reference) antibodies. (B) Δ ORD recruits VAP-A and excludes p150^{Glued} from RILP-Rab7 complexes. Me1JuSo cells expressing GFP-RILP and mRFP- Δ ORD, -ORP1L or - Δ ORDPHDPHD (as indicated) were fixed and stained for p150^{Glued} and VAP-A respectively. The different antigens are indicated. Zoom: overlay in three colours of CFP-RILP (blue), mRFP-ORP1L constructs (red) and YFP-VAP-A (in green). $n > 100$ for each condition. Scale bars, 10 μ m. (C) ORP1L recruits VAP-A from the ER. PA-GFP tagged VAP-A in living Me1JuSo cells also expressing either mRFP-tagged Δ ORDPHDPHD, Δ ORD or ORP1L was photoactivated with a 405nm light to follow transport of ER located PA-GFP/VAP-A to late endosomes by time-lapse microscopy. Firstly, a z-stack of cells was made to identify a location for selective photoactivation of the ER pool of VAP-A. Left panel shows an x-y, x-z and y-z projection through the location of photoactivation (the 405nm laser spot position shown as a circle). Subsequently, the cells were followed by time-lapse confocal microscopy and various snapshots of the mRFP and GFP channels, prior and post-photoactivation of PA-GFP/VAP-A, are shown. Right panel is a zoom-in on late endosomes (indicated by the box) and merge of the mRFP and GFP channel. $n > 10$ for each condition. Scale bars, 10 μ m. Movies are shown in Supplemental M2-4. (D) In vitro protein reconstitution experiment. Top: GTP-locked His-Rab7(Q67L) was coupled to TALON-beads and loaded with GTP before any of the isolated proteins indicated below were added to form another complex. After washing, these complexes were exposed to isolated VAP-A or the 150^{Glued}(C25) fragment, as indicated, and the effects on the pre-formed complex assessed by SDS-PAGE and Western blot analyses with specific antibodies, as indicated. A representative example of duplicate independent experiments is shown. Bottom: GST or GST-VAP-A were coupled to GST beads before exposure to the p150^{Glued}(C25) fragment. After washing, the complexes were analyzed by SDS-PAGE and Western blotting.



by ORP1L—binding to a more general receptor spectrin β III (Johansson et al., 2007). Both receptors are required for active dynein motor driven transport to the microtubule minus-end. Motor activities switch rapidly as visualized by the bidirectional motion of late endosomes. This switching is usually preceded by a ‘stop’ or immobile phase. Since the stop-time is rather variable, this is probably not a timely controlled process. The majority of the vesicles move in one line (supposedly the same microtubule) but another fraction continues under a different angle apparently switching mi-

cro-tubules. This suggests that vesicles do not switch direction by the same motor. We tested whether the mechanism of directional switching could be controlled by inactivating the Rab7 GTPase by TBC1D15. The Rab7 GAP TBC1D15 was identified using shRNA silencing of potential candidates in combination with photobleaching experiments to visualize the GFP-Rab7 GTPase cycle in living cells. However, RILP inhibited stimulation of the already low intrinsic Rab7 GTPase activity by TBC1D15, possibly by sharing overlapping binding sites with TBC1D15 in activated Rab7 (Figure

S2). Consequently, Rab7GAP cannot be responsible for the swift mechanism of the directional switching in late endosomal transport. Rab7-RILP has been identified as the late endosomal/lysosomal receptor for the p150^{Glued}-dynein motor. Since ORP1L also binds Rab7-RILP (Johansson et al., 2007), we tested whether this protein could control dynein motor binding to RILP. Using intramolecular FRET, we showed that the C-terminal ORD of ORP1L senses cholesterol in late endosomes resulting in a conformational change. Removal of the ORD prevents p150^{Glued} binding to RILP whereas a further 11 kDa C-terminal truncation (aa 408-514 in ORP1L) restored this binding. These data suggest that variations in late endosomal cholesterol levels elicit conformational changes in ORP1L which orchestrate motor protein binding. When the ORD is membrane-associated to bind cholesterol, the FFAT motif-containing ORP1L region preceding the ORD (aa 408-514 in ORP1L) allows binding of p150^{Glued} to RILP. Conversely, when the ORD is in its cytosolic orientated state or absent (as in the truncation mutant Δ ORD), the 11 kDa region preceding the ORD (aa 408-514) prevents access of p150^{Glued}-dynein motor complexes to Rab7-RILP. Thereby, vesicles disperse by moving to the microtubule plus-end. This 11 kDa region is comprised of a predicted coiled-coil and a FFAT motif that is critical in preventing p150^{Glued} interactions in the Δ ORD mutant. The FFAT motif in the ORP1L homologue OSBP interacts with VAPs in the ER (Loewen and Levine, 2005; Loewen et al., 2003) and modifies protein and lipid export from the ER (Wyles et al., 2002) and mutations in VAP-B cause familial amyotrophic lateral sclerosis (ALS) type 8 (Nishimura et al., 2004). Given the location in the ER, VAP would not be an obvious candidate for regulation of late endosomal transport, but we show VAP-A and -B accumulation on late endosomes driven by Δ ORD (that exposes the FFAT motif) but not Δ ORDPHDPHD

(where FFAT is inaccessible). In addition, we showed using photoactivation, that ER-located VAP-A travels to late endosomes but the exact transport pathway has not been resolved yet. Given the rapid transport and Brefeldin A-insensitivity (not shown), this unlikely is the result of classical transport through the Golgi. ORP1L may then interact in transit with VAP or actively recruit VAP from the ER membrane to control the dynein motor on late endosomes. Silencing VAP restores p150^{Glued} binding to Δ ORD-Rab7-RILP vesicles, suggesting that VAP is directly involved in removal of this dynein-dynactin motor subunit from the Rab7-RILP complex. This was confirmed using isolated proteins where purified VAP-A removed p150^{Glued} from the RILP-Rab7-ORP1L complex (which also indicated that we have identified the minimal unit of proteins in this process). These experiments furthermore showed that ORP1L is not required for executing removal of p150^{Glued} from the Rab7-RILP complex by VAP (in *in vitro* conditions), and that VAP directly interacts with the C-terminal segment of p150^{Glued}. However, cholesterol-dependent distinct ORP1L conformations determine VAP recruitment to the Rab7-RILP-p150^{Glued} complex and subsequent removal of p150^{Glued} from the Rab7-RILP receptor. This mechanism may be more general than described here, since the ORP1L homologue OSBP also uses VAP to modify ER export (Wyles et al., 2002), which is also driven by the dynein-dynactin motor complex. The motor receptor is unknown in this case. Whether other vesicles use sensors for cholesterol and VAP to control the dynein-dynactin motor, remains to be established.

When NPC1 is depleted, as in Niemann-Pick type C disease (Carstea et al., 1997), or when chemical drugs raise late endosomal cholesterol levels (Roff et al., 1991; Sobo et al., 2007), the ORD of ORP1L is membrane-associated excluding VAP. This allows enduring binding of p150^{Glued}-dynein motors

7

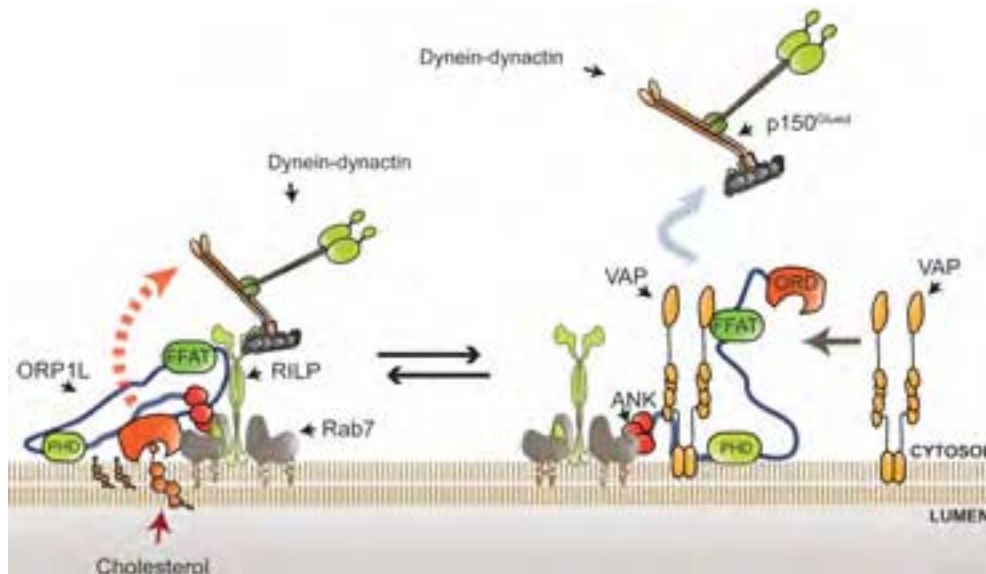


Figure 7. How cholesterol controls ORP1L conformations, VAP recruitment and p150^{Glued}-dynein motor binding to late endosomal Rab7-RILP receptors. Rab7 recruits the homodimeric effector RILP to late endosomes and lysosomes. The p150^{Glued} subunit of the dynein-dynactin motor directly interacts with RILP. ORP1L binds to the Rab7-RILP complex. Reciprocal ORP1L conformations reflect the C-terminal cholesterol-sensing domain of ORP1L (ORD) associated to cholesterol on the cytosolic leaflet of late endosomal membranes (left) or otherwise cytosolic (right). In the latter case, the FFAT motif preceding the ORD is exposed and recruits VAP. VAP binds to and removes p150^{Glued} from the Rab7-RILP receptor thus preventing minus-end transport and resulting in centrifugal translocation of late endosomal compartments. Cholesterol levels in late endosomes thus determine the conformation of ORP1L and VAP recruitment resulting in scattering under cholesterol-poor conditions and clustering of cholesterol-laden late endosomes/lysosomes, as in Niemann-Pick type C disease.

complexes to Rab7-RILP and transport to the microtubule minus-end. Cholesterol depletion results in microtubule plus-end transport of late endosomes unless the cholesterol-insensitive ORP1L variant ΔORD-PHDPHD is expressed. The positioning of vesicles bearing this chimera is independent of cholesterol levels as these remain densely clustered even when cholesterol-levels are lowered in late endosomes.

This mechanism explains how late endosomal cholesterol levels are associated with late endosomal positioning through cholesterol orchestrated recruitment of VAP by ORP1L that controls the Rab7-RILP-p150^{Glued}-dynein motor interaction (Fig 7). Since overexpression of ORP1L or ΔORD-

PHDPHD did not affect late endosomal cholesterol levels, ORP1L apparently uses local cholesterol levels (at the cytosolic leaflet of late endosomal membranes) as a messenger rather than actively contributing to cholesterol distribution in cells. Why cholesterol is selected for this purpose rather than lysobisphosphatidic acid (LBPA) or other lipids or molecules specific for late endosomes (Gruenberg and Stenmark, 2004), is unclear. It may be that cholesterol represents one of the few molecules present in the interior as well as the cytosolic leaflet of late endosomes allowing cytosolic exposure of intraluminal conditions. If cholesterol levels increase with maturation of late endosomes and lysosomes, the resulting ORP1L con-

trolled Rab7-RILP-p150^{Glued}-dynein motor interactions would position the most mature compartments at the extreme minus-end of microtubules with ‘shells’ of less mature vesicles surrounding these at more plus-end locations. Newly arriving late endosomes would then first encounter the ‘youngest’ late endosomes automatically resulting in spatial maturation before encountering lysosomes. Cholesterol would thus control the positioning of these organelles.

We have visualized how the Rab7-RILP complex controls transport of late endosomes. This process is controlled by cholesterol levels that direct ORP1L. The cholesterol-interacting protein ORP1L has two conformational states dependent on late endosomal cholesterol content and determines the dynein motor interaction with Rab7-RILP by selectively exposing its FFAT motif. The cytosolic exposed FFAT motif recruits VAP from the ER membrane. VAP then interacts with and removes the p150^{Glued} dynein motor subunit from the Rab7-RILP receptor of late endosomal and lysosomal membranes (Figure 7). This explains why cholesterol depletion causes late endosomal scattering and why high cholesterol levels induce lysosomal clustering, as observed in Niemann-Pick type C disease. Cholesterol in late endosomes is a messenger sensed by ORP1L to recruit VAP that binds to and removes dynein-dynactin motor complexes from late endosomal Rab7-RILP receptors and thus controls transport.

EXPERIMENTAL PROCEDURES

DNA constructs, Reagents and Antibodies

Rab7, RILP, VAP-A, VAP-B, p150^{Glued}(C25) and ORP1L cDNA constructs have been described previously (Johansson et al., 2007; Jordens et al., 2001; Marsman et al., 2004; Wyles et al., 2002). GFP, mRFP, GST, MBP and His-tagged constructs were constructed by PCR modification and cloning and described in Supplemental Experimental

Procedures. All constructs were sequenced verified and controlled by Western blot analyses. Reagents for manipulation of cellular cholesterol levels, cholesterol staining with filipin and antibodies for protein isolation, Western blotting and fluorescence microscopy are described in Supplemental Experimental Procedures.

Protein isolation and reconstitution studies

All proteins were expressed in E.coli with the exception of His-TBC1D15 that was isolated from 293T cells. Details on production and isolation are in Supplemental Experimental Procedures. Removal of GST from GST-VAP-A was by thrombin-cleavage followed by PMSF-precipitation of thrombin. The proteins were further purified by a GST-column and the flow-through contained GST-free VAP-A. Purity and correct molecular weight of the fusion proteins was controlled by SDS-PAGE and Coomassie staining. Proteins were stored in 8.7% glycerol at -80°C until use in protein reconstitution experiments. For Rab7GAP experiments, His-Rab7 was loaded with [γ -³²P]GTP before addition of His-RILP and GST-ORP1L in different combinations. His-TBC1D15 was added before the reaction was transferred from 4°C to 25°C. [γ -³²P]GTP-labelled His-Rab7 and [γ -³²P]GTP was precipitated by active charcoal unlike released ³²P-label which was quantified by scintillation counting. For in vitro effects of VAP-A on the ORP1L-Rab7-RILP-C25 protein complex, the GTPase-deficient His-Rab7(Q67L) was loaded onto TALON-beads and loaded with GTP (Sigma). Subsequently, the complex was formed by adding one or more of the following purified proteins: GST-ORP1L, His-RILP, MBP-p150^{Glued}(C25) and/or VAP-A. The complex was washed before addition of purified VAP-A or MBP-p150^{Glued}(C25) for 30 min at 20°C. Beads were washed before analysis by SDS-PAGE and Western Blotting. Alternatively, GST-VAP-A or purified GST were loaded onto GST-beads before ad-

dition of p150^{Glued}(C25) for 30 min at 20°C. After washing the beads were analyzed by SDS-PAGE and Western Blotting. Details are described in Supplemental Experimental Procedures.

Microscopy

Three and four-colour images on fluorescent fixed-samples were made using rabbit and mouse primary antibodies and mRFP- and GFP-labelled proteins. Images are made using Leica confocal laser scanning microscopes. Time-lapse imaging and Fluorescence Recovery After Photobleaching (FRAP) experiments were performed on a Leica TCS SP2 microscope equipped with a 37°C culture chamber. Vesicle motility analysis was performed using images analyzed by recovery curves of the time-lapse images which were generated using the MATLAB plug-in curve fitting toolbox. Photoactivation experiments were performed using a 405 nm laser on a Leica AOBIS system equipped with a 37°C culture chamber. Movies were made using IMAGE J programming. Lifetime imaging were taken on a Leica inverted DM-IRE2 microscope equipped with a Lambert Instruments (LI) frequency domain lifetime attachment (Leutingewolde, The Netherlands), controlled by the manufacturers' LI FLIM software. This microscopy was also equipped with a 37°C culture chamber. Filipin signal was recorded using a 365 nm excitation filter with 397 nm long pass emission using a Zeiss Axiovert 200 microscope equipped with an AxioCam CCD camera and a 20x Achromplan Ph2 dry lens. For further details on microscopy and data analyses, see Supplemental Experimental Procedures.

ACKNOWLEDGEMENTS

We thank K. Jalink for support with FLIM measurements and V. Olkkonen and M. Johansson for ORP1L reagents and constructs; N. Ridgway, M. Hardy, K. Ettayebi, and C. Hoogenraad for VAP-A and -B reagents.

We thank W. Moolenaar, H. Pickersgill and V. Menendez-Benito for critically reading the manuscript and S. Krom for helping with experiments. Nuno Rocha was supported by a Portuguese Foundation for Science and Technology FCT/ FSE PhD scholarship within the Third Framework Program. This work was supported by grants from the Dutch Cancer Society KWF and the Chemical Sciences Section of NWO.

REFERENCES

- Albert, S., Will, E., and Gallwitz, D. (1999). Identification of the catalytic domains and their functionally critical arginine residues of two yeast GTPase-activating proteins specific for Ypt/Rab transport GTPases. *Embo J* 18, 5216-5225.
- Bernards, A. (2003). GAPs galore! A survey of putative Ras superfamily GTPase activating proteins in man and Drosophila. *Biochim Biophys Acta* 1603, 47-82.
- Bornig, H., and Geyer, G. (1974). Staining of cholesterol with the fluorescent antibiotic "filipin". *Acta Histochem* 50, 110-115.
- Brown, C.L., Maier, K.C., Stauber, T., Ginkel, L.M., Wordeman, L., Vernos, I., and Schroer, T.A. (2005). Kinesin-2 is a motor for late endosomes and lysosomes. *Traffic* 6, 1114-1124.
- Bucci, C., Thomsen, P., Nicoziani, P., McCarthy, J., and van Deurs, B. (2000). Rab7: a key to lysosome biogenesis. *Mol Biol Cell* 11, 467-480.
- Burkhardt, J.K., Echeverri, C.J., Nilsson, T., and Vallee, R.B. (1997). Overexpression of the dynamitin (p50) subunit of the dynactin complex disrupts dynein-dependent maintenance of membrane organelle distribution. *J Cell Biol* 139, 469-484.
- Calleja, V., Ameer-Beg, S.M., Vojnovic, B., Woscholski, R., Downward, J., and Larijani, B. (2003). Monitoring conformational changes of proteins in cells by fluorescence lifetime imaging microscopy. *Biochem J* 372, 33-40.
- Carstea, E.D., Morris, J.A., Coleman, K.G.,

- Loftus, S.K., Zhang, D., Cummings, C., Gu, J., Rosenfeld, M.A., Pavan, W.J., Krizman, D.B., et al. (1997). Niemann-Pick C1 disease gene: homology to mediators of cholesterol homeostasis. *Science* 277, 228-231.
- Chen, H., Yang, J., Low, P.S., and Cheng, J.X. (2008). Cholesterol level regulates endosome motility via Rab proteins. *Biophys J* 94, 1508-1520.
- Chen, W., Sun, Y., Welch, C., Gorelik, A., Leventhal, A.R., Tabas, I., and Tall, A.R. (2001). Preferential ATP-binding cassette transporter A1-mediated cholesterol efflux from late endosomes/lysosomes. *J Biol Chem* 276, 43564-43569.
- Deacon, S.W., Serpinskaya, A.S., Vaughan, P.S., Lopez Fanarraga, M., Vernos, I., Vaughan, K.T., and Gelfand, V.I. (2003). Dynactin is required for bidirectional organelle transport. *J Cell Biol* 160, 297-301.
- Echard, A., Jollivet, F., Martinez, O., Lacapere, J.J., Rousselet, A., Janoueix-Lerosey, I., and Goud, B. (1998). Interaction of a Golgi-associated kinesin-like protein with Rab6. *Science* 279, 580-585.
- Förster, T. (1948). Zwischenmolekulare energiewanderung und fluoreszenz. *Annalen Physik* 6, 55-75.
- Gennerich, A., Carter, A.P., Reck-Peterson, S.L., and Vale, R.D. (2007). Force-induced bidirectional stepping of cytoplasmic dynein. *Cell* 131, 952-965.
- Gross, S.P., Welte, M.A., Block, S.M., and Wieschaus, E.F. (2002). Coordination of opposite-polarity microtubule motors. *J Cell Biol* 156, 715-724.
- Gruenberg, J., and Stenmark, H. (2004). The biogenesis of multivesicular endosomes. *Nat Rev Mol Cell Biol* 5, 317-323.
- Hamamoto, I., Nishimura, Y., Okamoto, T., Aizaki, H., Liu, M., Mori, Y., Abe, T., Suzuki, T., Lai, M.M., Miyamura, T., et al. (2005). Human VAP-B is involved in hepatitis C virus replication through interaction with NS5A and NS5B. *Journal of virology* 79, 13473-13482.
- Harada, A., Takei, Y., Kanai, Y., Tanaka, Y., Nonaka, S., and Hirokawa, N. (1998). Golgi vesiculation and lysosome dispersion in cells lacking cytoplasmic dynein. *J Cell Biol* 141, 51-59.
- Harrison, R.E., Bucci, C., Vieira, O.V., Schroer, T.A., and Grinstein, S. (2003). Phagosomes fuse with late endosomes and/or lysosomes by extension of membrane protrusions along microtubules: role of Rab7 and RILP. *Mol Cell Biol* 23, 6494-6506.
- Hoepfner, S., Severin, F., Cabezas, A., Habermann, B., Runge, A., Gillooly, D., Stenmark, H., and Zerial, M. (2005). Modulation of receptor recycling and degradation by the endosomal kinesin KIF16B. *Cell* 121, 437-450.
- Hollenbeck, P.J., and Swanson, J.A. (1990). Radial extension of macrophage tubular lysosomes supported by kinesin. *Nature* 346, 864-866.
- Holthuis, J.C., and Levine, T.P. (2005). Lipid traffic: floppy drives and a superhighway. *Nat Rev Mol Cell Biol* 6, 209-220.
- Holtta-Vuori, M., Maatta, J., Ullrich, O., Kuismanen, E., and Ikonen, E. (2000). Mobilization of late-endosomal cholesterol is inhibited by Rab guanine nucleotide dissociation inhibitor. *Curr Biol* 10, 95-98.
- Ikonen, E. (2008). Cellular cholesterol trafficking and compartmentalization. *Nat Rev Mol Cell Biol* 9, 125-138.
- Im, Y.J., Raychaudhuri, S., Prinz, W.A., and Hurley, J.H. (2005). Structural mechanism for sterol sensing and transport by OSBP-related proteins. *Nature* 437, 154-158.
- Infante, R.E., Abi-Mosleh, L., Radhakrishnan, A., Dale, J.D., Brown, M.S., and Goldstein, J.L. (2008a). Purified NPC1 protein. I. Binding of cholesterol and oxysterols to a 1278-amino acid membrane protein. *J Biol Chem* 283, 1052-1063.
- Infante, R.E., Radhakrishnan, A., Abi-Mosleh, L., Kinch, L.N., Wang, M.L., Grishin, N.V., Goldstein, J.L., and Brown, M.S. (2008b). Purified NPC1 protein: II. Localization of sterol binding to a 240-amino acid soluble luminal loop. *J Biol Chem* 283,

1064-1075.

- Johansson, M., Lehto, M., Tanhuanpää, K., Cover, T.L., and Olkkonen, V.M. (2005). The oxysterol-binding protein homologue ORP1L interacts with Rab7 and alters functional properties of late endocytic compartments. *Mol Biol Cell* 16, 5480-5492.
- Johansson, M., Rocha, N., Zwart, W., Jordens, I., Janssen, L., Kuijl, C., Olkkonen, V.M., and Neefjes, J. (2007). Activation of endosomal dynein motors by stepwise assembly of Rab7-RILP-p150Glued, ORP1L, and the receptor betaIII spectrin. *J Cell Biol* 176, 459-471.
- Jordens, I., Fernandez-Borja, M., Marsman, M., Dusseljee, S., Janssen, L., Calafat, J., Janssen, H., Wubbolts, R., and Neefjes, J. (2001). The Rab7 effector protein RILP controls lysosomal transport by inducing the recruitment of dynein-dynactin motors. *Curr Biol* 11, 1680-1685.
- Jordens, I., Marsman, M., Kuijl, C., and Neefjes, J. (2005). Rab proteins, connecting transport and vesicle fusion. *Traffic* 6, 1070-1077.
- Jordens, I., Westbroek, W., Marsman, M., Rocha, N., Mommaas, M., Huizing, M., Lambert, J., Naeyaert, J.M., and Neefjes, J. (2006). Rab7 and Rab27a control two motor protein activities involved in melanosomal transport. *Pigment Cell Res* 19, 412-423.
- King, S.J., Brown, C.L., Maier, K.C., Quinlyne, N.J., and Schroer, T.A. (2003). Analysis of the dynein-dynactin interaction in vitro and in vivo. *Mol Biol Cell* 14, 5089-5097.
- Koh, C.H., and Cheung, N.S. (2006). Cellular mechanism of U18666A-mediated apoptosis in cultured murine cortical neurons: bridging Niemann-Pick disease type C and Alzheimer's disease. *Cell Signal* 18, 1844-1853.
- Lebrand, C., Corti, M., Goodson, H., Cosson, P., Cavalli, V., Mayran, N., Faure, J., and Gruenberg, J. (2002). Late endosome motility depends on lipids via the small GTPase Rab7. *Embo J* 21, 1289-1300.
- Lehto, M., Hynynen, R., Karjalainen, K., Kuismanen, E., Hyvarinen, K., and Olkkonen, V.M. (2005). Targeting of OSBP-related protein 3 (ORP3) to endoplasmic reticulum and plasma membrane is controlled by multiple determinants. *Exp Cell Res* 310, 445-462.
- Lehto, M., Mayranpää, M.I., Pellinen, T., Ihalmo, P., Lehtonen, S., Kovanen, P.T., Groop, P.H., Ivaska, J., and Olkkonen, V.M. (2008). The R-Ras interaction partner ORP3 regulates cell adhesion. *J Cell Sci* 121, 695-705.
- Lemmon, M.A., and Ferguson, K.M. (2000). Signal-dependent membrane targeting by pleckstrin homology (PH) domains. *Biochem J* 350 Pt 1, 1-18.
- Loewen, C.J., and Levine, T.P. (2005). A highly conserved binding site in vesicle-associated membrane protein-associated protein (VAP) for the FFAT motif of lipid-binding proteins. *J Biol Chem* 280, 14097-14104.
- Loewen, C.J., Roy, A., and Levine, T.P. (2003). A conserved ER targeting motif in three families of lipid binding proteins and in Opi1p binds VAP. *Embo J* 22, 2025-2035.
- Ma, S., and Chisholm, R.L. (2002). Cytoplasmic dynein-associated structures move bidirectionally in vivo. *J Cell Sci* 115, 1453-1460.
- Marsman, M., Jordens, I., Kuijl, C., Janssen, L., and Neefjes, J. (2004). Dynein-mediated vesicle transport controls intracellular Salmonella replication. *Mol Biol Cell* 15, 2954-2964.
- Maxfield, F.R., and Tabas, I. (2005). Role of cholesterol and lipid organization in disease. *Nature* 438, 612-621.
- Mobius, W., van Donselaar, E., Ohno-Iwashita, Y., Shimada, Y., Heijnen, H.F., Slot, J.W., and Geuze, H.J. (2003). Recycling compartments and the internal vesicles of multivesicular bodies harbor most of the cholesterol found in the endocytic pathway. *Traffic* 4, 222-231.
- Mukherjee, S., and Maxfield, F.R. (2004). Lipid and cholesterol trafficking in NPC.

- Biochim Biophys Acta 1685, 28-37.
- Muller, M.J., Klumpp, S., and Lipowsky, R. (2008). Tug-of-war as a cooperative mechanism for bidirectional cargo transport by molecular motors. *Proc Natl Acad Sci U S A* 105, 4609-4614.
- Narita, K., Choudhury, A., Dobrenis, K., Sharma, D.K., Holicky, E.L., Marks, D.L., Walkley, S.U., and Pagano, R.E. (2005). Protein transduction of Rab9 in Niemann-Pick C cells reduces cholesterol storage. *Faseb J* 19, 1558-1560.
- Nishimura, A.L., Mitne-Neto, M., Silva, H.C., Richieri-Costa, A., Middleton, S., Cascio, D., Kok, F., Oliveira, J.R., Gillingwater, T., Webb, J., et al. (2004). A mutation in the vesicle-trafficking protein VAPB causes late-onset spinal muscular atrophy and amyotrophic lateral sclerosis. *American journal of human genetics* 75, 822-831.
- Nishimura, Y., Hayashi, M., Inada, H., and Tanaka, T. (1999). Molecular cloning and characterization of mammalian homologues of vesicle-associated membrane protein-associated (VAMP-associated) proteins. *Biochemical and biophysical research communications* 254, 21-26.
- Patel, S.C., Suresh, S., Kumar, U., Hu, C.Y., Cooney, A., Blanchette-Mackie, E.J., Neufeld, E.B., Patel, R.C., Brady, R.O., Patel, Y.C., et al. (1999). Localization of Niemann-Pick C1 protein in astrocytes: implications for neuronal degeneration in Niemann-Pick type C disease. *Proc Natl Acad Sci U S A* 96, 1657-1662.
- Pepperkok, R., Squire, A., Geley, S., and Bastiaens, P.I. (1999). Simultaneous detection of multiple green fluorescent proteins in live cells by fluorescence lifetime imaging microscopy. *Curr Biol* 9, 269-272.
- Peterson, M.R., and Emr, S.D. (2001). The class C Vps complex functions at multiple stages of the vacuolar transport pathway. *Traffic* 2, 476-486.
- Pfeffer, S.R. (2001). Rab GTPases: specifying and deciphering organelle identity and function. *Trends Cell Biol* 11, 487-491.
- Rink, J., Ghigo, E., Kalaidzidis, Y., and Zerial, M. (2005). Rab conversion as a mechanism of progression from early to late endosomes. *Cell* 122, 735-749.
- Roff, C.F., Goldin, E., Comly, M.E., Cooney, A., Brown, A., Vanier, M.T., Miller, S.P., Brady, R.O., and Pentchev, P.G. (1991). Type C Niemann-Pick disease: use of hydrophobic amines to study defective cholesterol transport. *Dev Neurosci* 13, 315-319.
- Ross, J.L., Wallace, K., Shuman, H., Goldman, Y.E., and Holzbaun, E.L. (2006). Processive bidirectional motion of dynein-dynactin complexes in vitro. *Nat Cell Biol* 8, 562-570.
- Seals, D.F., Eitzen, G., Margolis, N., Wickner, W.T., and Price, A. (2000). A Ypt/Rab effector complex containing the Sec1 homolog Vps33p is required for homotypic vacuole fusion. *Proc Natl Acad Sci U S A* 97, 9402-9407.
- Shaner, N.C., Campbell, R.E., Steinbach, P.A., Giepmans, B.N., Palmer, A.E., and Tsien, R.Y. (2004). Improved monomeric red, orange and yellow fluorescent proteins derived from *Discosoma* sp. red fluorescent protein. *Nature biotechnology* 22, 1567-1572.
- Sobo, K., Le Blanc, I., Luyet, P.P., Fivaz, M., Ferguson, C., Parton, R.G., Gruenberg, J., and van der Goot, F.G. (2007). Late endosomal cholesterol accumulation leads to impaired intra-endosomal trafficking. *PLoS ONE* 2, e851.
- Stinchcombe, J.C., Majorovits, E., Bossi, G., Fuller, S., and Griffiths, G.M. (2006). Centrosome polarization delivers secretory granules to the immunological synapse. *Nature* 443, 462-465.
- Suchanek, M., Hynynen, R., Wohlfahrt, G., Lehto, M., Johansson, M., Saarinen, H., Radzikowska, A., Thiele, C., and Olkkonen, V.M. (2007). The mammalian oxysterol-binding protein-related proteins (ORPs) bind 25-hydroxycholesterol in an evolutionarily conserved pocket. *Biochem J* 405, 473-480.
- Sugii, S., Lin, S., Ohgami, N., Ohashi, M.,

- Chang, C.C., and Chang, T.Y. (2006). Roles of endogenously synthesized sterols in the endocytic pathway. *J Biol Chem* 281, 23191-23206.
- Vaughan, P.S., Leszyk, J.D., and Vaughan, K.T. (2001). Cytoplasmic dynein intermediate chain phosphorylation regulates binding to dynactin. *J Biol Chem* 276, 26171-26179.
- Wubbolts, R., Fernandez-Borja, M., Jordens, I., Reits, E., Dusseljee, S., Echeverri, C., Vallee, R.B., and Neefjes, J. (1999). Opposing motor activities of dynein and kinesin determine retention and transport of MHC class II-containing compartments. *J Cell Sci* 112 (Pt 6), 785-795.
- Wubbolts, R., Fernandez-Borja, M., Oomen, L., Verwoerd, D., Janssen, H., Calafat, J., Tulp, A., Dusseljee, S., and Neefjes, J. (1996). Direct vesicular transport of MHC class II molecules from lysosomal structures to the cell surface. *J Cell Biol* 135, 611-622.
- Wurmser, A.E., Sato, T.K., and Emr, S.D. (2000). New component of the vacuolar class C-Vps complex couples nucleotide exchange on the Ypt7 GTPase to SNARE-dependent docking and fusion. *J Cell Biol* 151, 551-562.
- Wyles, J.P., McMaster, C.R., and Ridgway, N.D. (2002). Vesicle-associated membrane protein-associated protein-A (VAP-A) interacts with the oxysterol-binding protein to modify export from the endoplasmic reticulum. *J Biol Chem* 277, 29908-29918.
- Yang, H. (2006). Nonvesicular sterol transport: two protein families and a sterol sensor? *Trends Cell Biol* 16, 427-432.
- Zerial, M., and McBride, H. (2001). Rab proteins as membrane organizers. *Nat Rev Mol Cell Biol* 2, 107-117.
- Zhang, X.M., Walsh, B., Mitchell, C.A., and Rowe, T. (2005). TBC domain family, member 15 is a novel mammalian Rab GTPase-activating protein with substrate preference for Rab7. *Biochemical and biophysical research communications* 335, 154-161.

SUPPLEMENTAL EXPERIMENTAL PROCEDURES

Reagents

Rabbit anti-GFP and rabbit anti-mRFP antibodies were generated using purified His-mRFP or His-GFP recombinant proteins as immunogens, respectively. Cross-reactivity was excluded by Western blot analyses with various mRFP- or GFP-labelled fusion proteins. Rabbit polyclonal anti-NPC1 was from Novus Biologicals, Inc. (Littleton, CO, USA), rat monoclonal anti-tubulin antibody was from Abcam plc (Cambridge, UK), rabbit anti-human VAP antiserum was a kind gift of Dr. N. Ridgway (Dalhousie University, Canada). Rabbit-anti HA tag was from Santa Cruz. Fluorescent secondary antibodies were from Molecular Probes.

Lovastatin (or Mevinolin) was purchased from Calbiochem (Darmstadt, Germany) and converted from its inactive prodrug form to its open acid form prior to use, by first dissolving the prodrug in ethanol and heating to 50°C for 2 hr in NaOH. Sodium-phosphate buffer was then added and this solution was heated to 40°C for 30 min. Finally, the pH was adjusted to 7.3 with concentrated HCl. Mevalonate was prepared by dissolving Mevalonolactone (Sigma-Aldrich, Schnellendorf, Germany) in a 0.05 M NaOH solution. The pH was adjusted to 7.0 with 0.1 M HCl.

U18666A (Calbiochem) was dissolved in ethanol to a final concentration of 10 mg/ml.

The lipoprotein-deficient serum (LPDS) was prepared as described (Goldstein et al., 1983) and was a kind gift from Dr. M. Jauhainen at the National Public Health Institute (Helsinki, Finland).

cDNA constructs and vectors

Rab7, RILP and ORP1L cDNA constructs have been described previously (Johansson et al., 2007; Jordens et al., 2001; Marsman et al., 2004). GST-VAP-A was a kind gift from

Dr. M. Hardy and K. Ettayebi (Montana State University, USA) and HA-VAP-A and HA-VAP-B from Dr. C. Hoogenraad (Teuling et al., 2007). VAP-A was cut with BamHI and XhoI and cloned into both a pAGFP-C1 vector and an YFP-C1 vector (using the BglII and SalI sites). GFP-ANKPHD and mRFP-ANKPHD were generated by subcloning the ANKPHD fragment from pCDNA4-ANKPHD (Johansson et al., 2007) into a pEGFP-C1 (BD Biosciences Clontech, USA) or into a custom made pmRFP-C1 vector (Johansson et al., 2007), respectively, using the BamHI and XbaI sites.

Δ ORD was generated by PCR using primers 5'-ACTCGGATCCATGAACA-CAGAAGCGGAGCAACA-3' and 5'-AAAGGATCCCTATCTGTGTTTTC-TACTGCCCAAATGC-3' and inserted into the BamHI site of pcDNA4HisMax-C (Invitrogen) and the BglII site of pmRFP-C1 (Johansson et al., 2007) vectors.

To generate mRFP- Δ ORDPHD, mRFP- Δ ORD was digested with XbaI and EcoRI. The remainder of Δ ORD was amplified by PCR using primers 5'-CTCAAATGATTAAGGAGTGTGACATGGCTA-3' and 5'-CCGGAATTCCATTCTGTGTTTTCTACTGCCCAAATGCTC-3'. The amplified fragment was inserted into the XbaI and EcoRI sites of the previously digested mRFP- Δ ORD vector. The first PH domain was generated by PCR using primers 5'-CCGGAATTCCGATATGAGGGCCCTCTCTGGAAGA-3' and 5'-CGGGGTACCGCTGTAAGCAGAATGTTCTTCTATTGC-3' and ligated into the EcoRI and KpnI sites. Subsequently, the second PH domain was also generated by PCR using primers 5'-CGGGGTACCGATATGAGGGCCCTCTCTGGAAGA-3' and 5'-CGGGATCCATTCTAGCTGTAAGCAGAATGTTCTTCTATTGC-3' and inserted using the KpnI and BamHI sites.

mRFP- Δ ORDFFAT(D478A) was generated by PCR using mRFP- Δ ORD as template and 5'-CCCAGAATTCTATGCG-

GCGCTGTCAGATTCCGAGTC-3' and 5'-AAGCAAGTAAAACCTCTACAAATG-3' as primers, followed by swapping of the wild-type FFAT motif in mRFP-ΔORD for the mutated FFAT using the EcoRI and BamHI restriction sites.

The ORP1L-FRET construct (mRFP-ORP1L-GFP) was generated in two steps. Firstly, mRFP-ORP1L was digested with NheI and SacI (internal site in ORP1L) which was subsequently cloned into pEGFP-N1 (Clontech) to obtain an N-terminal region of ORP1L which was N-terminally tagged to mRFP and C-terminally tagged to GFP. In the second step, the C-terminal part of ORP1L was produced by PCR using primers 5'-GGAGTGTGACATGGCTAA-3' and 5'-CGGGATTCCATAAATGTCAG-GCAAATTGAAG-3', mutating the ORP1L stop codon. The PCR product was digested using SacI and BamHI, and cloned into the intermediate construct described.

TBC1D15 was a kind gift from Xiang-Ming Zhang (Zhang et al., 2005). shRNA targeting TBC1D15 were made using the pSUPER vector system (Brummelkamp et al., 2002) and the sequences 5'-AATGGGACATGGTTAATACAGTT-3' and 5'-AAGGCATGAAGACCCAGCTAATT-3'. siRNA for human NPC1 was obtained from Dharmacon (ON-TARGETplus SMARTpool for accession no. NM_000271) and transfected using DharmaFECT 1 transfection reagent (Dharmacon).

All constructs were sequence verified. Expressed proteins had the expected molecular weight as confirmed by SDS-PAGE and Western blotting analyses.

Cell culture and drug treatment

Monolayers of MelJuSo cells were maintained in Iscoves Modified Dulbecco's Medium (IMDM) medium (Gibco) supplemented with 5% FCS, in 5% CO₂ at 37°C.

For S-medium treatment, MelJuSo cells were washed with PBS and then cultured in IMDM supplemented with 5% LPDS, 50 μM

lovastatin to inhibit HMG-CoA reductase, and 230 μM mevalonate to supply essential non-sterol isoprenoids for cell growth and survival (Liscum et al., 1989; Sugii et al., 2006), for 4 hr before analyses. For U-medium treatment, cells were washed with PBS and cultured in IMDM supplemented with 5% FCS and 3 μg/ml of U18666A for 15 hr before analyses.

Microscopy

Transfected cells were fixed at 48 hr (DNA), 48 hr (RNAi) or 72 hr (RNAi and DNA) post-transfection with 4% formaldehyde in PBS for 30 min and permeabilized for 5 min with 0.05% Triton X-100 in PBS, at room temperature. Nonspecific binding of antibodies was blocked by 0.5% BSA/PBS for 40 min, after which cells were incubated with a primary antibody in 0.5% BSA/PBS for 1 hr at room temperature. Bound primary antibodies were visualized with Alexa Fluor secondary antibody conjugates (Invitrogen). Cells were mounted in Vectashield mounting medium (Vector Laboratories, USA). The specimens were analyzed with confocal laser scanning microscopes (TCS-SP1, -SP2 or AOBS) equipped with HCX PL APO 63x/NA 1.32 and HCX PL APO lbd. bl 63x/NA 1.4 oil-corrected objective lenses (all from Leica, Mannheim, Germany). The acquisition software used was Leica LCS.

Live imaging of MelJuSo cells stably expressing GFP-MHC class II (Wubboldt et al., 1999) was performed on a Leica TCS SP2 System (Leica, Mannheim, Germany) at 37°C in a 5% CO₂ culture hood surrounding the objective stage of the microscope. Vesicle movement was analyzed with the ImageJ plugin "Manual Tracking". Obtained tracking data was further processed in Microsoft Excel. The angle between vectors was calculated using the following formula:

$$\cos\theta = \frac{a_1b_1 + a_2b_2}{|A||B|}$$

FRAP experiments were performed as described previously (Jordens et al., 2001; Reits et al., 2000). Briefly, MelJuSo cells expressing GFP-Rab7 were microinjected with constructs expressing an shRNAi targeting a GAP protein. Approximately 24 hr after microinjection GFP-Rab7 vesicles were bleached with a high-intensity laser beam. Subsequently, the recovery of fluorescence in the bleached spot was quantified. Lysosomes and late endosomes with little lateral movement were selected. Because the vesicles were not completely stationary, their position was tracked and intensity measured by a program written in Matlab (Mathworks, Natick, MA) and the percentage of fluorescence recovery after 200 s was determined. Independent experiments were analyzed. Photo-activation experiments were performed in MelJuSo cells transfected with photo-activatable GFP tagged to VAP-A, cotransfected with mRFP-tagged-ORP1L, -ORP1LAORD or -ORP1LAORDPDHPDH. Cells were mounted in phenol-red-free DMEM (Invitrogen), limiting medium autofluorescence. All measurements were performed on a Leica AOBs system equipped with a 37°C culture chamber and HCX PL APO lbd.bl 63x/NA 1.4 oil-corrected objective lenses. Cells were imaged using a 488 nm and 561 nm laser, to visualize the activated PA-GFP and mRFP tagged proteins, respectively. Point-activation with full power from the 405 nm laser was performed for 3 seconds at the nuclear region, where ER could be activated outside of the confocal plain. To prevent PA-GFP/VAP-A activation already present on late endosomal/lysosomal structures, a Z-stack was performed before activation.

Fluorescence Lifetime Imaging Microscopy (FLIM).

FLIM experiments were performed with MelJuSo cells stably expressing GFP-ORP1L-mRFP cultured on Delta T dishes (Bi-optechs). Prior to measurements, cells were

mounted in bicarbonate-buffered saline medium (140 mM NaCl, 5 mM KCl, 2 mM MgCl₂, 1 mM CaCl₂, 23 mM NaHCO₃, 10 mM [D-]glucose, and 10 mM Hepes, pH 7.3) and analyzed at 37°C in a 5% CO₂ culture hood surrounding the objective stage of the microscope. Images were taken on a Leica inverted DM-IRE2 microscope with a HCX PL APO 63x/NA 1.35 glycerol corrected objective lens equipped with a Lambert Instruments (LI) frequency domain lifetime attachment (Leutingewolde, The Netherlands), controlled by the manufacturer's LI FLIM software. GFP was excited with ~4 mW of 488 nm light from a LED modulated at 40 MHz, and emission was collected at 490–550 nm using an intensified charge-coupled device camera (CoolSNAP HQ; Roper Scientific). To calculate the GFP lifetime, the intensities from 12 phase-shifted images (modulation depth ~70%) were fitted with a sinus function, and lifetimes were derived from the phase shift between excitation and emission. For internal controls, cells were co-cultured with MelJuSo cells expressing H2B-GFP only. Lifetimes were referenced to a 1 μM solution of rhodamine-G6 in saline that was set at a 4.11 ns lifetime. The donor FRET efficiency E_D was calculated as $E_D = 1 - (\text{measured lifetime}/\text{GFP lifetime in control cells})$ (Zwart et al., 2005).

Filipin stainings.

Filipin staining was performed on formaldehyde fixed cells for 2 hr at room temperature with 0.05 mg/ml freshly dissolved filipin (Sigma) in PBS supplemented with 0.5 % BSA, and imaged using a Zeiss Axiovert 200 microscope equipped with an AxioCam CCD camera and a 20 x Achroplan Ph2 dry lens. Filipin signal was recorded using a 365 nm excitation filter with 397 nm long pass emission. mRFP signal was recorded with a 546 nm excitation filter with 590 nm long pass emission (Zeiss). For data acquisition, the manufacturers' software was used.

Protein purification.

His-Rab7, His-RILP, and GST-ORP1L were produced as previously described (Johansson et al., 2007). His-tagged mTBC1D15 was purified from human HEK293T cells. Cells were lysed in 0.5% Triton X-100, 20 mM Hepes (pH 7.5), 200 mM NaCl, 8 mM β -mercaptoethanol and Complete EDTA-free Protease Inhibitors Cocktail (Roche Diagnostics). The lysates was cleared by centrifugation and the supernatant was incubated with preequilibrated Talon Co^{2+} resin (Clontech Laboratories, Inc.) for 30 min. The resin was then washed extensively with 20 mM Hepes (pH7.5), 200 mM NaCl and 8 mM β -mercaptoethanol. His-tagged mTBC1D15 was eluted with washing buffer supplemented with 500 mM imidazole. The purity and concentration of the eluted protein was determined by SDS-PAGE and Coomassie staining. GST-VAP-A construct in pGEX was a kind gift of Dr. N. Ridgway (Wyles et al., 2002). GST was removed by cleavage with thrombin by incubation at 30°C for 2 hr before inactivation and precipitation by 0.1mM PMSF. GST was removed by glutathione beads and purity of the free VAP-A was checked by SDS-PAGE and Coomassie staining.

In vitro GTPase assay.

The GTPase assay was performed as described previously (Askjaer et al., 1999). Briefly, His-Rab7 was loaded with [γ - ^{32}P]GTP (10 mCi/ml, >5000 Ci/mmol, Amersham) in the presence of 10 mM EDTA. Loading as stopped by adding MgCl_2 to a concentration of 20 mM followed by gel filtration on a Bio-Spin 6 column (BioRad) equilibrated with buffer (0.1 M Tris-HCl pH 7.5, 10 mM MgCl_2 , 2 mM dithiothreitol, 0.5 M NaCl). Reaction mixtures containing [γ - ^{32}P]GTP Rab7 were pre-incubated with GST-ORP1L (3 μM) and/ or His-RILP (3 μM) in reaction buffer (40 mM Tris-HCl [pH 8.0], 50 mM NaCl, 8 mM MgCl_2 , 1 mM DTT, 0.5 mM GTP, 0.1 mg/ml BSA, 1 mM

phosphate, 1% glycerol) on ice for 10 min. To test the accessibility of TBC1D15 towards Rab7 in complex with ORP1L and/or RILP, His-tagged TBC1D15 (0.9 μM) was added to the reaction mixture. Reactions were incubated at 25°C and stopped after 15 min by addition of 1 ml of charcoal suspension (7% w/v charcoal, 10% v/v ethanol, 0.1 M HCl, 10 mM KH_2PO_4) (Bischoff and Pongstingl, 1995). The mixture was centrifuged for 2 min in a tabletop centrifuge. Release of free [^{32}P]ortho-phosphate was determined by scintillation counting in the supernatant.

In vitro motor removal by and binding to VAP-A.

The reconstitution assay was performed in a detergent/salt buffer (20 mM Hepes, pH 7.5, 200 mM NaCl, 4 mM β -mercaptoethanol, 5 mM MgCl_2 , 0.05% [vol/vol] Triton X-100, and 50 μM GTP). 15 μg His-Rab7(Q67L) was coupled to 3 μl TALON beads and pre-loaded with GTP. Beads were washed to remove unbound His-Rab7(Q67L) and recombinant purified His-RILP (3 μg), GST-ORP1L (8.7 μg), VAP-A (2.2 μg) and MBP-p150^{Glued}(C25) (4.5 μg) were added to the beads as indicated and incubated in a total volume of 0.4 ml for 2 h at 4°C. Beads were washed extensively and MBP-p150^{Glued}(C25) (4.5 μg) or VAP-A (2.2 μg) was added to the beads as indicated. Proteins were subsequently incubated in a total volume of 0.4 ml of detergent/salt buffer for 30 min at 22°C. Beads were washed extensively and proteins bound to His-Rab7(Q67L) were analyzed by SDS-PAGE and Western blotting. Proteins were detected with the following antibodies: α -His (Amersham Biosciences), α -MBP (New England Biolabs), α -GST (kind gift of W. Moolenaar, NKI, Amsterdam). Direct binding of p150^{Glued} to VAP-A was assayed as follows. 30 μg GST-VAP-A or 15 μg GST was coupled to 15 μl glutathione-Sepharose 4B beads. Beads were washed to remove unbound proteins, and MBP-p150^{Glued}(C25) (4.5 μg) was added to the beads in a total

volume of 0.4 ml for 30 min at 22°C. Beads were washed extensively and proteins bound to the glutathione-Sepharose 4B beads were analyzed by SDS-PAGE and Western blotting.

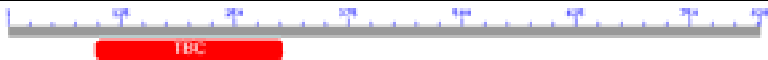




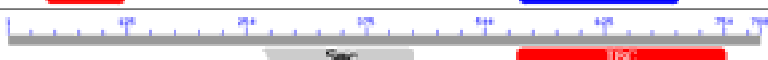

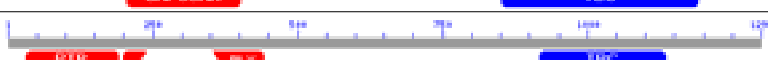
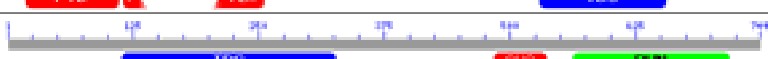
References.

- Askjaer, P., Bachi, A., Wilm, M., Bischoff, F.R., Weeks, D.L., Ogniewski, V., Ohno, M., Niehrs, C., Kjems, J., Mattaj, I.W., et al. (1999). RanGTP-regulated interactions of CRM1 with nucleoporins and a shuttling DEAD-box helicase. *Mol Cell Biol* 19, 6276-6285.
- Bischoff, F.R., and Ponstingl, H. (1995). Catalysis of guanine nucleotide exchange of Ran by RCC1 and stimulation of hydrolysis of Ran-bound GTP by Ran-GAP1. *Methods Enzymol* 257, 135-144.
- Brummelkamp, T.R., Bernards, R., and Agami, R. (2002). A system for stable expression of short interfering RNAs in mammalian cells. *Science* 296, 550-553.
- Goldstein, J.L., Basu, S.K., and Brown, M.S. (1983). Receptor-mediated endocytosis of low-density lipoprotein in cultured cells. *Meth Enzymol* 98, 241-260.
- Johansson, M., Rocha, N., Zwart, W., Jordens, I., Janssen, L., Kuijl, C., Olkkonen, V.M., and Neefjes, J. (2007). Activation of endosomal dynein motors by stepwise assembly of Rab7-RILP-p150Glued, ORP1L, and the receptor betaIII spectrin. *J Cell Biol* 176, 459-471.
- Jordens, I., Fernandez-Borja, M., Marsman, M., Dusseljee, S., Janssen, L., Calafat, J., Janssen, H., Wubbolts, R., and Neefjes, J. (2001). The Rab7 effector protein RILP controls lysosomal transport by inducing the recruitment of dynein-dynactin motors. *Curr Biol* 11, 1680-1685.
- Liscum, L., Ruggiero, R.M., and Faust, J.R. (1989). The intracellular transport of low density lipoprotein-derived cholesterol is defective in Niemann-Pick type C fibroblasts. *J Cell Biol* 108, 1625-1636.
- Marsman, M., Jordens, I., Kuijl, C., Janssen, L., and Neefjes, J. (2004). Dynein-mediated vesicle transport controls intracellular Salmonella replication. *Mol Biol Cell* 15, 2954-2964.
- Reits, E.A., Vos, J.C., Gromme, M., and Neefjes, J. (2000). The major substrates for TAP in vivo are derived from newly synthesized proteins. *Nature* 404, 774-778.
- Sugii, S., Lin, S., Ohgami, N., Ohashi, M., Chang, C.C., and Chang, T.Y. (2006). Roles of endogenously synthesized sterols in the endocytic pathway. *J Biol Chem* 281, 23191-23206.
- Teuling, E., Ahmed, S., Haasdijk, E., Demmers, J., Steinmetz, M.O., Akhmanova, A., Jaarsma, D., and Hoogenraad, C.C. (2007). Motor neuron disease-associated mutant vesicle-associated membrane protein-associated protein (VAP) B recruits wild-type VAPs into endoplasmic reticulum-derived tubular aggregates. *J Neurosci* 27, 9801-9815.
- Wubbolts, R., Fernandez-Borja, M., Jordens, I., Reits, E., Dusseljee, S., Echeverri, C., Vallee, R.B., and Neefjes, J. (1999). Opposing motor activities of dynein and kinesin determine retention and transport of MHC class II-containing compartments. *J Cell Sci* 112 (Pt 6), 785-795.
- Wyles, J.P., McMaster, C.R., and Ridgway, N.D. (2002). Vesicle-associated membrane protein-associated protein-A (VAP-A) interacts with the oxysterol-binding protein to modify export from the endoplasmic reticulum. *J Biol Chem* 277, 29908-29918.
- Zhang, X.M., Walsh, B., Mitchell, C.A., and Rowe, T. (2005). TBC domain family, member 15 is a novel mammalian Rab GTPase-activating protein with substrate preference for Rab7. *Biochem Biophys Res Commun* 335, 154-161.

Supplemental Movies can be found on: <http://publications.labstore.nl>

Supplemental Figure S1

Supplemental Table a

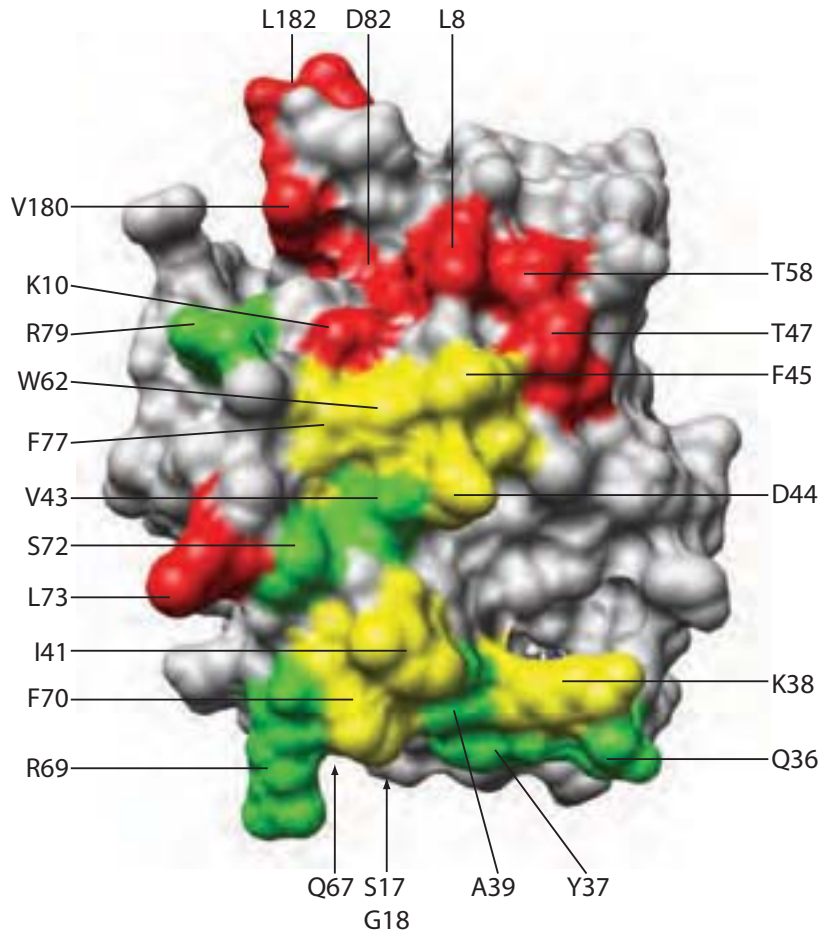
Symbol	Domain(s)
USP6NL (RNTRE)	
TBC1D17	
TBC1D15	
TBC1D5	
TBC1D2	
TBC1D2B	
RABGAP1L	
TBC1D4 (AS160)	
SGSM3	

Supplemental Table b

Symbol	shRNAi sequences
USP6NL (RNTRE)	AAGTCACAGATAGATTTGGCTTT AAAGCTTAAAGATGAGGCAGATT
TBC1D17	AATTCCCCCTTCCCAGATGTCCTT
TBC1D15	AATGGGACATGGTTAATACAGTT AAGGCATGAAGACCCAGCTAATT
TBC1D5	AAGGTTGTTGGCCAACAAGATTT AACTGTAGCACCTATAGTCTTT
TBC1D2	AAGCCTTCTCTGACCATCAGTTT AAGGTGGTGTTCGCTATGCCTT
TBC1D2B	AAATTCATTAAATTTTACTCTT AAGTACAAGGAAGAGGAGATTTT
RABGAP1L	AAAAACCTCAACTGAAGATAGTT AAAGGCCAAGCAGTCTTCTTGTT
TBC1D4 (AS160)	AACAGCCACGACCTCACCTACTT AATGTGAGAGCTTTGAAAATATT
SGSM3	AACCCCTTGGTGGCCCTGTGTT AAGTGTACCAGCCCTGGTCTCTT

Supplemental Figure S1. Table a: Domain structure of the nine potential Rab GTPase GAPs tested by shRNA-mediated silencing. Name (Symbol), domain structure (Domain(s)) and size (numbers indicate amino acid residues) are indicated. The TBC domain is typical for GAPs for Rab GTPases. Table b: Sequences of primers cloned into pSUPER used for silencing of potential GAP proteins.

Supplemental Figure S2



The crystal structure of Rab7 interacting with RILP or TBC1D15.

Supplemental Figure S2. Overlapping interaction surfaces in GTP-Rab7 for TBC1D15 and RILP. Residues interacting with RILP are coloured red. The interaction with RILP is based on the crystal structure of the RILP-Rab7 complex (Wu et al., 2005). Residues predicted to interact with TBC1D15 are coloured green. The prediction is based on the structure of GYP1 and Rab33 (Pan et al., 2006). Given that both TBC1D15 and GYP1 contain a conserved TBC domain which interacts with the cognate GTPase, the interaction of TBC1D15 with Rab7 is likely similar to that of GYP1 with Rab33. Residues shared by RILP and TBC1D15 are coloured yellow.

The large surface area predicted to be shared between RILP and TBC1D15 suggests that binding of RILP to Rab7 will prevent binding of TBC1D15. In this way, RILP not only locks Rab7 in the GTP-bound active state (Marsman et al., 2006), but also prevents access of the GTPase-activating protein TBC1D15.